Atmos. Chem. Phys., 13, 6165–6184, 2013
www.atmos-chem-phys.net/13/6165/2013/
doi:10.5194/acp-13-6165-2013

Atmospheric Chemistry and Physics Open Access

Measurements of OVOC fluxes by eddy covariance using a proton-transfer-reaction mass spectrometer – method development at a coastal site

M. Yang[1], **R. Beale**[1], **T. Smyth**[1], **and B. Blomquist**[2]

[1]Plymouth Marine Laboratory, Prospect Place, Plymouth, Devon, UK
[2]University of Hawaii, Department of Oceanography, Honolulu, HI, USA

Correspondence to: M. Yang (miya@pml.ac.uk)

Received: 7 October 2012 – Published in Atmos. Chem. Phys. Discuss.: 26 March 2013
Revised: 29 May 2013 – Accepted: 30 May 2013 – Published: 1 July 2013

Abstract. We present here vertical fluxes of oxygenated volatile organic compounds (OVOCs) measured with eddy covariance (EC) during the period of March to July 2012 near the southwest coast of the United Kingdom. The performance of the proton-transfer-reaction mass spectrometer (PTR-MS) for flux measurement is characterized, with additional considerations given to the homogeneity and stationarity assumptions required by EC. Observed mixing ratios and fluxes of OVOCs (specifically methanol, acetaldehyde, and acetone) vary significantly with time of day and wind direction. Higher mixing ratios and fluxes of acetaldehyde and acetone are found in the daytime and from the direction of a forested park, most likely due to light-driven emissions from terrestrial plants. Methanol mixing ratio and flux do not demonstrate consistent diel variability, suggesting sources in addition to plants. We estimate air–sea exchange and photochemical rates of these compounds, which are compared to measured vertical fluxes. For acetaldehyde, the mean (1σ) mixing ratio of 0.13 (0.02) ppb at night may be maintained by oceanic emission, while photochemical destruction outpaces production during the day. Air–sea exchange and photochemistry are probably net sinks of methanol and acetone in this region. Their nighttime mixing ratios of 0.46 (0.20) and 0.39 (0.08) ppb appear to be affected more by terrestrial emissions and long-distance transport, respectively.

1 Introduction

Oxygenated volatile organic compounds (OVOCs), such as methanol, acetone, and acetaldehyde, exist ubiquitously in the troposphere. Methanol is the most abundant oxygenated organic gas in the atmosphere and a source of carbon monoxide (Duncan et al., 2007) and formaldehyde (Millet et al., 2006). Plant growth is a large source of methanol (Guenther et al., 2000; Galbally and Kirstine, 2002), accounting for 30–80 % of total emissions to the atmosphere in global models (Singh et al., 2000; Heikes et al., 2002; Jacob et al., 2005; Millet et al., 2008). Other sources include plant decay (Warneke et al., 1999), industrial emissions (such as solvents, fuel additive, antifreeze, etc.; Langford et al., 2009), and atmospheric reactions such as the oxidation of methane. In addition to consumption by the hydroxyl radical (OH), methanol is removed from the planetary boundary layer (PBL) via deposition to land (Karl et al., 2004) and to the ocean surface (Heikes et al., 2002; Williams et al., 2004; Carpenter et al., 2004), resulting in an overall atmospheric lifetime of about 4.7 days globally (Millet et al., 2008).

Acetaldehyde is important for the formation of tropospheric ozone (O_3), HO_x radicals (Singh et al., 1995), and peroxyacetyl nitrate (Roberts, 1990), the latter a stable reservoir of nitrogen oxides. While terrestrial plants are well known to emit acetaldehyde (Guenther et al., 2000; Jardine et al., 2008), a recent mesocosm measurement in a Norwegian fjord suggests that the ocean could be a source as well (Sinha et al., 2007). In the updated global budget by Millet et al. (2010), hydrocarbon oxidation in the atmosphere represents the predominant source of acetaldehyde (60 %),

more than 3 times higher than a previous estimate (Singh et al., 2004); other sources include emissions from the ocean (27 %) and terrestrial biosphere (11 %), as well as minor anthropogenic contributions. Acetaldehyde is quickly removed from air via reactions with OH, the nitrate radical, and direct photolysis (Atkinson, 2000), with an overall lifetime of ~ 0.8 days globally (Millet et al., 2010).

A significant source of OH radical in the dry upper troposphere, acetone is also a precursor to peroxyacetyl nitrate (Singh et al., 1995). Direct emissions from plants (Warneke et al., 1999; Guenther et al., 2000) and indirect photochemical oxidations provide similar contributions to the global acetone budget (Fischer et al., 2012), while anthropogenic emission appears to be a minor source (Langford et al., 2009). Reaction with OH, photolysis, and deposition to land are the main sinks of atmospheric acetone, resulting in an overall lifetime of 14 days globally (Fischer et al., 2012). Global budgets of acetone disagree on the role of the ocean. Jacob et al. (2002) suggested the ocean to be a net source, whereas Singh et al. (2004) modeled a net loss of acetone to the sea surface. With eddy covariance, Marandino et al. (2005) measured an oceanic uptake of acetone over the North Pacific; though for the tropical Pacific, measured and predicted acetone fluxes opposed in sign. Other observations over the ocean (Taddei et al., 2009) and in the mesocosm (Sinha et al., 2007) indicated the air–sea flux of acetone to be small and variable in direction.

With developments in mass spectrometry over the last two decades, OVOC concentrations have been measured in a variety of environments (though few by the coast). The numerous sources and sinks pose considerable challenges to the characterization and modeling of OVOC cycling based on concentrations alone. Knowing the vertical transport allows emission and deposition to be distinguished from chemical transformation, which represents a significant step forward, particularly for understanding the role of the ocean. Moreover, when multiple OVOCs are measured simultaneously, commonality and difference in the sources and sinks may be inferred.

Eddy covariance (EC) is the most direct technique for measuring vertical transport in the atmosphere. Vertical flux (F) is derived by correlating fluctuations in the species of interest (x) with concurrent vertical wind velocity (w) and averaging over time ($F = \overline{w'x'}$). When measured within the surface layer of the atmosphere ($< \sim 10$ % of the PBL), the EC flux can be equated to surface flux under stationary and horizontally homogeneous conditions. Statistical measures of x in time and space, stationarity and homogeneity refer to temporal constancy during the averaging period and spatial constancy within the flux footprint. For methanol, acetaldehyde, and acetone, the stationarity criterion (i.e., steady state) should be satisfied from the perspective that their chemical lifetimes are much longer than the flux averaging period of typically an hour.

To capture the full continuum of atmospheric turbulence, a fast sensor (typically with frequency $f \geq 10$ Hz) is required. Capable of sampling at > 1 Hz, the proton-transfer-reaction mass spectrometer (PTR-MS) has been utilized to measure OVOC fluxes in terrestrial environments with EC (e.g., Karl et al., 2001). To accommodate the lower sampling frequency of the PTR-MS when multiple compounds are simultaneously monitored, disjunct (e.g., Rinne et al., 2001; Warneke et al., 2002) and virtual disjunct (e.g., Karl et al., 2002; Spirig et al., 2005) EC methods based on discrete mixing ratio measurements have also been used, albeit with greater flux loss at high frequencies.

Compared to terrestrial emissions, air–sea fluxes of OVOCs tend to be lower in magnitude, thus challenging the instrumental sensitivity and noise. In this paper, we first discuss the optimization of the PTR-MS for EC flux measurements of OVOCs, with detailed analysis of the sampling error, detection limit, and high-frequency flux loss. Additional attention is given to the interpretation of flux measurements with regard to the homogeneity and stationarity requirements. Lastly, we compare measured vertical fluxes to expected air–sea exchange and photochemical rates.

2 Measurement site and environmental conditions

The city of Plymouth (population of $\sim 250\,000$) is situated on the SW coast of the United Kingdom. Warmed by the North Atlantic Current, the region has a temperate oceanic climate and is predominantly exposed to southwesterly winds. As shown in Fig. 1, Plymouth Marine Laboratory (PML, 50°21.57′ N, 4°08.52′ W) is located on the northern side of Plymouth Sound, which opens to the Atlantic Ocean to the south and is fed by the River Plym from the NE and Tamar from the NW (both estuarine). Mount Edgcumbe Park, abundant with broadleaf trees and grasses, is situated ~ 2 km SW of PML and across the Tamar. Residential buildings, a commercial ferry port, and a naval dockyard are located NW of PML, while the city center is to the NE.

Measurements of OVOC mixing ratios and winds were made from the rooftop of the PML building, which is 200–300 m from the water's edge (depending on direction). A parking area fenced by broadleaf trees and garden bushes occupies the ~ 80 m region immediately south of PML, with a tall hotel across the parking area severely obstructing winds from the SSE. The view is much clearer from south to west, with moderately dense, two- to three-storey residential buildings covering most of the land that slopes steeply down to the water's edge. The rooftop of the PML building is about 45 m above sea level and 15 m above local ground level. Taking 10 m to be the height of the roughness elements (e.g., houses, trees) above sea level, the roughness sublayer height can be approximated as 3 times the height of the roughness elements, or 30 m (World Meteorological Organization, 2006). Thus the PML rooftop should be above the roughness

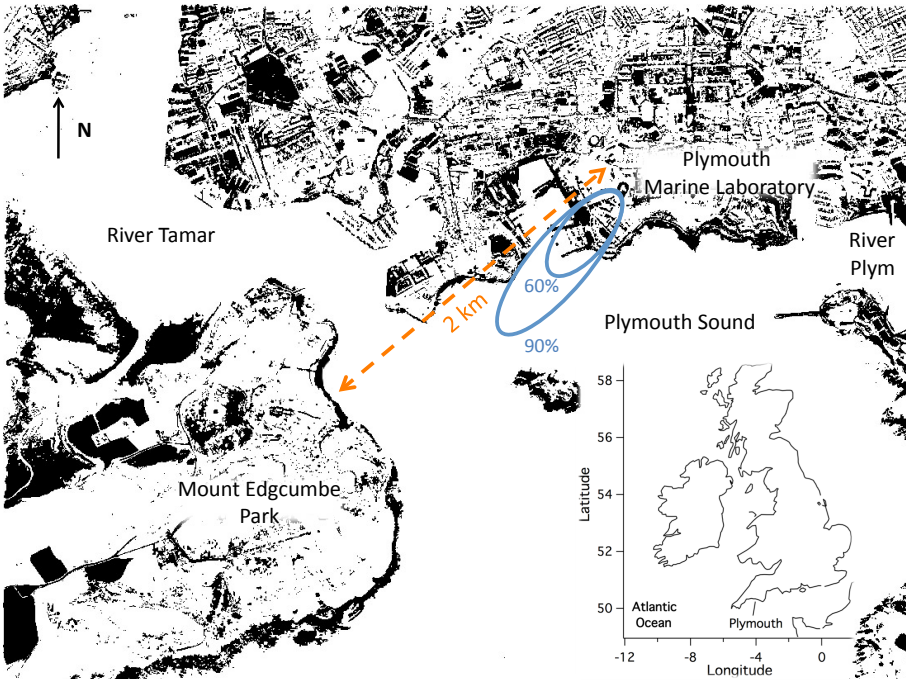

Fig. 1. Map of Plymouth Sound and the location of Plymouth. The small and large ellipses illustrate the approximated 60 % and 90 % (cumulative) flux footprint under typical conditions. At ∼ 2 km SW of the PML and separated by the River Tamar, the forested Mount Edgcumbe Park likely lies outside of the flux footprint.

sublayer and within the surface layer, where standard boundary layer theory applies.

For descriptions of the regional environment, we utilize continuous observations from the PML rooftop, Rame Head, and L4 buoy, all parts of the Western Channel Observatory. Meteorological parameters were measured every 5 min from a station secured on a ∼ 2 m mast near the SW corner of the PML rooftop, including horizontal wind speed and direction (Mierji Meteo solid-state wind sensor, MMW-005), temperature and humidity (Hygroclip S3 sensor), precipitation (Omni Instruments 15 cm tipping bucket rain gauge, RG200), solar irradiance (Li-Cor pyranometer, LI-200SZ), and photosynthetically active radiation (Chelsea Instruments half-hemisphere PAR sensor). Meteorological data were also recorded every 5 min from Rame Head, a headland several km SW of PML (50°19.03′ N, 4°13.19′ W). Just outside of Plymouth Sound, the autonomous L4 buoy (50°15.0′ N, 4°13.0′ W) is equipped with sensors that measure surface ocean parameters hourly, including chlorophyll *a* from fluorescence (WetLabs WQM), nitrate (Satlantic ISUS), sea surface temperature, salinity, etc.

We report here OVOC fluxes measured during selected periods between March and July 2012. Due to unusually rainy weather, high winds, and larger riverine inputs of nutrients, the "spring" bloom of phytoplankton was almost continuous during these months, with a mean chlorophyll *a* mixing ratio of $\sim 1.7\,\mathrm{mg\,m^{-3}}$. Sea surface temperature steadily warmed from approximately 10 to 15 °C, while salinity dropped from 35.2 to 35.0 psu. Under typical southwesterly conditions, the flux footprint (the area contributing to the measured turbulent fluxes) extends to ∼ 1 km upwind of PML, covering both land and coastal waters (described in detail in Sect. 5.2).

3 Instrumentation and basic data processing

A high-sensitivity PTR-MS (Ionicon Analytik) was used to measure the mixing ratios of selected OVOCs. The gas inlet and a 3-D sonic anemometer (Applied Technologies, Inc., "K" style probe) were installed near the SE corner of the rooftop of the PML building. To keep out rain droplets, the gas inlet was constructed with two opposing funnels with mouths held together, sandwiching a coarse mesh. Stabilized by an aluminum rod on the exterior, the inlet pointed downwards and was located ∼ 40 cm below and 30 cm in front of the sonic center (of the w component). Around 25 m of perfluoroalkoxy (Teflon PFA) tubing (6.4 mm inner diameter (ID)) linked the inlet to the PTR-MS in a laboratory two floors below. Turbulent airflow in the manifold (Reynolds number of ∼ 5000) was maintained at ∼ 25 standard liter per minute (SLPM) by a vacuum pump and monitored by a digital thermal mass flow meter (Bronkhorst EL-FLOW series). OVOC mixing ratio, wind, and flow data were recorded on the same computer.

We used an internal gas standard to account for instrumental drift in the PTR-MS. Triply deuterated (d_3) methanol diluted in nitrogen (1.01 ppm, Scientific and Technical Gases Ltd) was continuously injected into the manifold at about 2 m ahead of a subsampling "tee" for the PTR-MS via a short piece of 1.6 mm. ID fluorinated ethylene propylene (Teflon FEP) tubing. The standard flow was controlled precisely at 0.100 SLPM by a digital mass flow controller (Bronkhorst EL-FLOW series), yielding a diluted d_3 methanol mixing ratio of $\sim$ 4 ppb. At the tee, another short piece of 1.6 mm. ID FEP tubing was connected to a 3-way polytetrafluoroethylene (Teflon PTFE) solenoid valve (Takasago Electric, Inc.), which directed air either directly to the PTR-MS or additionally through a catalytic converter. The PTR-MS subsampled from the manifold at $\sim 60\,\mathrm{mL\,min^{-1}}$ via $\sim$ 1.5 m of 0.8 mm. polyether ether ketone (PEEK) tubing, which was heated to 80 °C to minimize adsorption. The residence time of air inside of the main manifold was about 2 s, and from the tee to the PTR-MS another $\sim$ 2 s. A higher subsampling flow by the PTR-MS may slightly improve the instrument response, but resulted in unstable chamber pressure in the current setup.

3.1 Optimization of the PTR-MS for eddy covariance

The principle of the PTR-MS was described in detail by Lindinger et al. (1998). Very briefly, from a water vapor source, the instrument produces the hydronium ion (H_3O^+) with a proton affinity (PA) of $691\,\mathrm{kJ\,mol^{-1}}$, which in turn transfers the charge to gas molecules of higher PA. With PA of 754, 769, and $812\,\mathrm{kJ\,mol^{-1}}$, methanol, acetaldehyde, and acetone are ionized efficiently by H_3O^+ to form ions at mass to charge ratio (m/z) of 33, 45, and 59, respectively.

High sensitivity and low noise are desirable for EC. In order to maintain H_3O^+ as the primary source ion, a low pressure in the drift tube (reaction chamber) is typically used in the PTR-MS (2–3 mbar), which limits the concentrations of analytes and so the frequency of molecular collisions. Increasing the chamber pressure may improve sensitivity, but can also lead to more dimerization of water molecules, which at a PA of $\sim 808\,\mathrm{kJ\,mol^{-1}}$ (Goebbert and Wentold, 2004) does not ionize many OVOCs efficiently. A large fraction of the m/z 33 background is due to the oxygen isotope $^{16}O^{17}O^+$, which relates to O^{2+} by the isotopic fraction of 0.076 %. The amount of O_2^+ in the system decreases with increasing humidity (de Gouw et al., 2004), implying that the m/z 33 background may be lowered by increasing H_3O^+ input. Doing so may also result in more water dimers, which can be broken by increasing the electric field or temperature in the reaction chamber. With aforementioned considerations, the following settings were typically used: drift tube pressure of 2.8 mbar, temperature of 80 °C, voltage of 700 V, and water vapor flow of 9 sccm. A substantially higher m/z 59 background was observed at chamber temperatures above 100 °C, presumably due to desorption. The electric field to charge ratio (E/N) was 112 Td at 298 K (and greater at 80 °C), high enough to avoid excessive clustering of water molecules (de Gouw et al., 2003).

OVOC backgrounds were quantified by diverting the gas flow through a platinum catalytic converter (Shimadzu) at 350 °C for 2 min at the beginning of every hour. The converter removes organic compounds but does not significantly alter signals at m/z 21 ($H_3^{18}O^+$), 32 (O_2^+), and 37 ($H_2O \cdot H_3O^+$). For m/z 33, 45, and 59, background values were typically 0.8, 0.3, and 0.2 ppb and generally stable (derivations of mixing ratios are described in Sect. 3.2). Estimated as 3σ of the 2 min backgrounds over a day, the detection limits for mean mixing ratios of these compounds were 0.048, 0.021, and 0.016 ppb.

To maintain a high enough sampling frequency for EC, we only monitored a few OVOC species simultaneously. Related to H_3O^+ by an isotopic ratio of 500, m/z 21 was measured at a dwell time of 50 ms, following by m/z 33, 36 (d_3 methanol), 45, and/or 59 at a dwell time of 100 ms each, resulting in a total sampling frequency of 2.1–2.5 Hz. While shorter dwell times would result in faster sampling, potential gain in speed is offset by amplified instrumental noise at ambient concentrations. On separate measuring or scan modes, m/z 32 and 37 were monitored occasionally, and represented less than 1 % and 5 % of the m/z 21 signal, respectively.

At a dwell time of 100 ms, instrumental noise is much higher than detection limit for mean mixing ratio. Estimated as 1σ of high-rate data during a period of background, the noise levels for m/z 33, 45, and 59 were 0.21, 0.13, and 0.10 ppb, which agree with statistical errors from a counting detector and are confirmed to be white noise from the variance spectra. The PTR-MS generally performed well during this period, with H_3O^+ of $2.5\text{–}3.0 \times 10^7$ counts per seconds (cps). Instrument sensitivities differed among OVOCs and improved somewhat with time, partly due to varying transmission efficiencies. From an hour after three days of continuous operation, sensitivities at m/z 33, 45, and 59 were 292, 456, and 511 cps $\mathrm{ppb^{-1}}$.

3.2 OVOC mixing ratios from PTR-MS

The PTR-MS converts the number of analyte molecules to a mixing ratio (C) through the concentration of air in the drift tube:

$$C = \frac{10^9}{[\mathrm{air}]} \frac{1}{k_{C+} \cdot t_{\mathrm{drift}}} \frac{\mathrm{cnts}_{C+}}{\mathrm{cnts}_{H_3O^+}} \frac{\mathrm{Tr}_{H_3O^+}}{\mathrm{Tr}_{C+}}. \quad (1)$$

The kinetic reaction rate, k_{C+}, depends on the chemical structure (dipole moment, polarizability, etc.) of the gas molecule (Zhao and Zhang, 2004). After subtracting the backgrounds, cnts_{C+} and $\mathrm{cnts}_{H_3O^+}$ are the signals of C^+ and H_3O^+ in cps. $\mathrm{Tr}_{H_3O^+}$ and Tr_{C+} indicate the respective transmission efficiencies of the PTR-MS, which depend on ion extraction efficiency to the quadrupole, and the efficiencies of the mass spectrometer and of the detector (Taipale et al.,

2008). Tr is mainly mass dependent, but also varies over time and from one instrument to another.

The reaction time between H_3O^+ and the analyte within the drift tube, t_{drift}, is short under our settings at only 94 µs:

$$t_{drift} = \frac{l^2}{\mu_0 U_{drift}} \frac{T_0}{T_{drift}} \frac{P_{drift}}{P_0}. \quad (2)$$

Here l is the length of the chamber (9 cm) and μ_0 the reduced mobility (2.8 $cm^2\ volt^{-1}\ s^{-1}$). U_{drift}, T_{drift}, and P_{drift} are the steadily maintained drift tube voltage, temperature, and pressure, and T_0 and P_0 the standard temperature and pressure. The actual residence time of air through the drift tube is much longer. Out of the 60 mL min^{-1} subsampling flow by the PTR-MS, roughly half goes through the drift tube, resulting in a residence time of ~ 0.1 s, which is one of the limitations to instrument frequency response.

In the field where temperature and humidity vary significantly, efficiency and performance of the PTR-MS can fluctuate as well. Thus empirical calibration factors need to be determined accurately and frequently for individual instruments using external gas standards, which is nontrivial. Alternatively, k_{C+} and Tr are not necessary for deriving ambient mixing ratio from an internal isotopic standard with similar molecular properties. Such should be the case for d_3 methanol, which is structurally similar to ambient methanol and only differs in mass by 3 amu. Analogous to how the University of Hawaii measures DMS (Blomquist et al., 2010), we derive the mixing ratio of ambient methanol ($C_{methanol}$) from the ratio between counts at m/z 33 and 36:

$$C_{methanol} = C_{methanol,std} \frac{cnts_{33}}{cnts_{36}} \frac{A_{36,std}}{A_{33,amb}}. \quad (3)$$

Calculated from the standard gas cylinder concentration and measured mass flow dilution rate, $C_{methanol,std}$ is the mixing ratio of d_3 methanol in the manifold. Because the d_3-methanol flow is essentially constant, we can remove counting noise from $cnts_{36}$ with a low-pass filter at a cutoff frequency of 0.017 Hz. The last ratio on the right-hand side (RHS) of Eq. (3) accounts for the distributions of isotopomers at m/z 33 and 36. $A_{36,std}$ indicates the isotopic ratio of m/z 36 in the gas standard cylinder, which was measured from mass scans to be 0.9925. $A_{33,amb}$ represents the isotopic ratio of m/z 33 in ambient air, which was estimated from natural abundance of elements to be 0.9860. Abundances of the deuterated isotopomer in ambient air and the undeuterated isotopomer in the standard are insignificant and neglected in this analysis.

We monitor slow drift in the PTR-MS from the ratio between ambient methanol mixing ratios determined from isotopic dilution and directly outputted by the instrument: $R_{33} = C_{methanol}/C_{33,PTR\text{-}MS}$. Here $C_{33,PTR\text{-}MS}$ was calculated from Eq. (1) assuming a reaction rate of $2.6 \times 10^{-9}\ cm^3\ s^{-1}$ (Zhao and Zhang, 2004) and instrument-specific transmission efficiencies. From two separate 3-day periods, the hourly averaged R_{33} ranged between 0.82 and 0.92, with a mean (1σ) of 0.87 (0.02). The use of Eq. (1) thus appears to overestimate methanol mixing ratio by 10–20 %, likely due to uncertainties and variability in k_{C+} and Tr. Without calibration standards for acetaldehyde and acetone for this period, we first used recommended k_{C+} from Zhao and Zhang (2004) to compute their mixing ratios following Eq. (1), and further corrected them for PTR-MS drift by applying the factor R_{33}. Such adjustments could introduce additional biases to mean mixing ratios, but should help preserving temporal trends. As with $cnts_{36}$ in Eq. (3), $cnts_{H_3O^+}$ was low-pass-filtered in Eq. (1).

3.3 Possible biases in the mixing ratio measurements

Because of the unit m/z resolution of the PTR-MS, different compounds very close in mass are not distinguished. Such is the case at m/z 59, where propanal and glyoxal can potentially interfere with the measurements of acetone. The PA of glyoxal is 675–691 kJ mol^{-1} according to theoretical calculations (Wróblewski et al., 2007), probably too low to be ionized effectively by H_3O^+. While the detection of propanal should be more efficient because of its greater PA at 784 kJ mol^{-1}, Warneke et al. (2003) suggested that due to its short atmospheric lifetime (~ 9 h), the background level of this compound should be low away from predominantly industrial sources.

Northway et al. (2004) suggested that heterogeneous reaction with O_3 on the inlet wall could lead to acetaldehyde formation, an artifact likely more severe for stratospheric air and for gas chromatography (Apel et al., 2008). Given our high manifold flow rate and short residence time, a large inlet-related artifact seems unlikely. O_3 mixing ratio measured at Rame Head was usually below 20 ppb, with a diurnal fluctuations of 4–5 ppb for SW winds. The lack of correlation between acetaldehyde and O_3 as well as the low magnitude and range in O_3 also do not support substantial heterogeneous production of acetaldehyde. Nevertheless, with potential artifacts and without specific internal standards, our measured mixing ratios of acetone and acetaldehyde are more uncertain.

3.4 General behaviors in OVOC mixing ratios

Mixing ratios of methanol, acetaldehyde, and acetone varied substantially due not only to local production and destruction, but also horizontal advective and turbulent transport. Figure 2 shows the OVOC mixing ratios vs. wind direction for 6–8 June, when a large low-pressure system passed by Plymouth, resulting in heavy precipitation at times and wind gusts up to 20 m s^{-1}. High winds and wet deposition likely reduced the PBL loadings of these OVOCs upwind, allowing observed mixing ratios to be more reflective of local changes. We separate mixing ratios to day (approximately 1 h after sunrise to 1 h before sunset) and night (1 h after sunset to

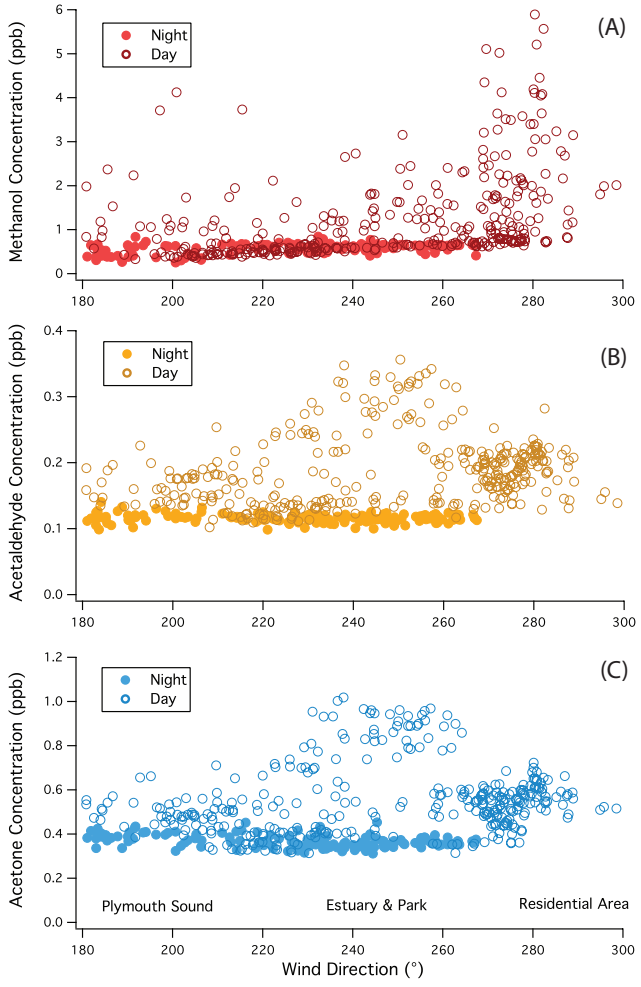

Fig. 2. Mixing ratios of methanol **(A)**, acetaldehyde **(B)**, and acetone **(C)** as a function of wind direction during the period 6–8 June. For acetaldehyde and acetone, mixing ratios were higher during the day than at night and demonstrated maxima in the direction of WSW (Mount Edgcumbe Park). Much higher methanol mixing ratios were observed during the day and typically from the NW.

1 h before sunrise). For methanol, the nighttime mixing ratio was ∼0.5 ppb and uniform with respect to wind direction. During the day, however, methanol mixing ratio ranged from ∼0.5 ppb to an order of magnitude higher; the latter generally occurred when winds were from the NW (the direction of residential buildings, a commercial ferry port, and a naval boatyard). Nighttime mixing ratios of acetaldehyde and acetone were also relatively steady at ∼0.1 and 0.4 ppb, independent of wind direction. In contrast, daytime mixing ratios of acetaldehyde and acetone were 2–3 times the nighttime values, peaking from WSW. The directional dependence suggests that the higher daytime values were related to surface sources rather than widespread photochemical production in the atmosphere.

Methanol generally showed more fluctuations on short timescales than acetone, likely due to greater strength and spatial heterogeneity of methanol sources. This is clearly visible during the period 3–4 March when winds were largely from the SW (Fig. 3). Despite similar mean mixing ratios of ∼0.4 ppb, σ in methanol mixing ratio (0.71) was about 5 times greater than that of acetone (0.13). If the fluctuations in mixing ratio were mainly from vertical turbulent transport, based on $F = \overline{w'x'}$, methanol flux should be several times larger than acetone flux, which we show to be the case in Sect. 5.1. OVOC mixing ratios were often substantially elevated when winds were weak (e.g., 03:00 to 06:00 UTC on 4 March). A shallow nocturnal boundary layer during this period probably concentrated these gases.

A time series of acetaldehyde mixing ratio during 15 June is shown in Fig. 4 along with solar irradiance. Whitecapping was clearly visible over Plymouth Sound on this day with strong winds (∼11 m s^{-1}) from the SSW. Atmospheric dimethyl sulfide (DMS) mixing ratio was also detected by the PTR-MS, which confirmed the marine influence. Consistent with previous diel cycle observations (e.g., Bandy et al., 1996; Yang et al., 2009), DMS mixing ratio decreased in the afternoon, when photochemical destruction outpaced sea-to-air emission, until a few hours before sunset. Contrastingly, acetaldehyde mixing ratio generally increased with solar irradiance.

Crudely, we approximate the nighttime mixing ratios of OVOCs from the wind sector of 180–270° to be their "baselines" for North Atlantic air, which for methanol, acetaldehyde, and acetone were 0.46 (0.20), 0.13 (0.02), and 0.39 (0.08) ppb (mean and 1σ from March to July). This methanol mixing ratio is similar to previous aircraft measurements over the Pacific (Singh et al., 2004), and ground-based observations from the marine sector at Mace Head, on the west coast of Ireland (Lewis et al., 2005). The acetone mixing ratio above is also comparable to those measured from the tropical Atlantic (Williams et al., 2004) and Mace Head (Lewis et al., 2005), but lower than values reported by Marandino et al. (2005) north of 25° N in the Atlantic. Any possible inlet-related artifact aside, 0.13 (0.02) ppb of acetaldehyde is on the lower end of previous nighttime marine air observations of typically 0.2–0.6 ppb by Zhou and Mopper (1993) from the Caribbean and 0.1–0.5 ppb by Lewis et al. (2005).

4 Eddy covariance flux calculations

Undisturbed atmospheric turbulence is critical for the EC method. The rooftop is admittedly not an ideal location because of potentially large distortion of airflow by the building superstructure. To best capture SW winds, we extended the sonic anemometer horizontally beyond the building wall by ∼2 m (to the south). Wind velocities in three axes (u, v, w) and temperature (T_S) were recorded by the anemometer at a frequency of 10 Hz. In our set up, u was along the NS direction, perpendicular to the wall, v along the EW direction, and w positive upwards, such that a positive flux indicates

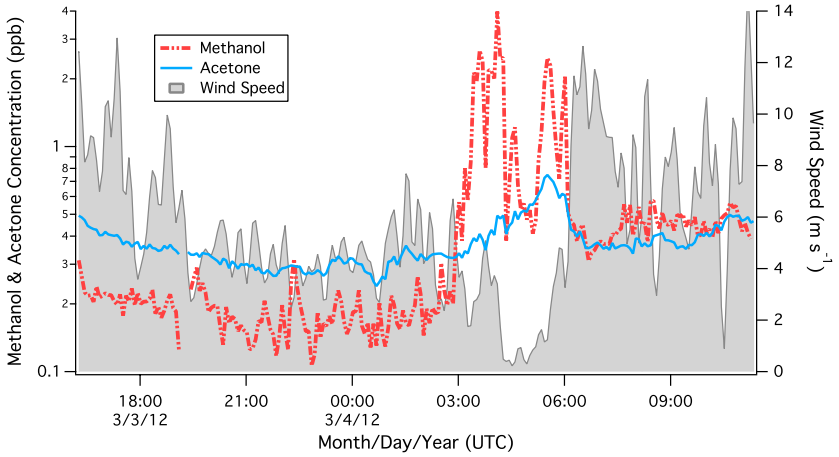

Fig. 3. Mixing ratios of methanol and acetone during the period 3–4 March, along with wind speed (from SW). Greater fluctuations were apparent in the mixing ratio of methanol than in acetone on short timescales, in part due to greater spatial heterogeneity of methanol sources. Methanol mixing ratio increased by an order of magnitude when the wind ceased, probably due to a shallow nocturnal boundary layer.

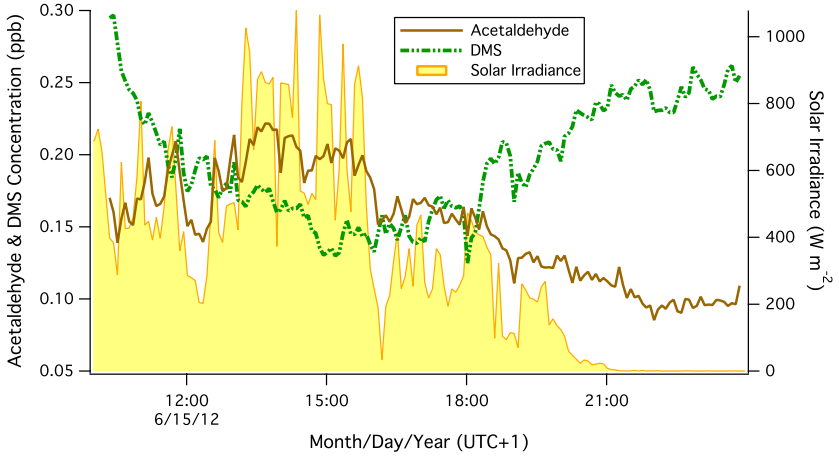

Fig. 4. Mixing ratios of acetaldehyde and DMS on 15 June, along with solar irradiance. With strong winds from SSW (over Plymouth Sound), DMS mixing ratio was detectable by the PTR-MS and demonstrated the expected diel variability, while acetaldehyde mixing ratio peaked in solar noon and declined for the rest of the daytime.

an upward transfer from the surface. The sonic anemometer temperature (T_s) was corrected for humidity to yield the air temperature (T_a). A standard double rotational correction was applied to u, v, and w to account for the streamline of airflow over the building superstructure. After rotation, both v and w averaged zero, while u aligned with the mean horizontal wind.

The severity of wind distortion is reflected in the tilt angle from the second rotation, which typically ranged from $\sim 10°$ for W winds to $\sim 20°$ for SW winds, as air was forced upwards when encountering the building. Distortion of airflow is also evident from the ratios in the variance spectra (S) between u, v, and w after rotation. In the inertial subrange ($> \sim 1$ Hz), both $S_w(f)/S_u(f)$ and $S_v(f)/S_u(f)$ should be $\sim 4/3$, which was indeed the case for westerly winds, implying minimally distorted flow. For SW winds, however, while $S_w(f)/S_u(f)$ remained at 4/3, $S_v(f)/S_u(f)$ was generally higher at ~ 1.5, indicating a greater flow distortion (increased variance) in the direction orthogonal to the mean horizontal wind. Fortunately, the computation of scalar fluxes only requires w, not u and v. Thus disturbance in the horizontal probably did not significantly bias OVOC fluxes, but may have contributed additional scatter. Despite the nonideal measuring location, wind direction from the sonic anemometer generally shows good agreement with the solid-state sensor from the PML rooftop and with the mechanical (cup) anemometer from Rame Head. Due to an instrument fault, one or two channels of the sonic anemometer sensor often outputted corrupted data during heavy rain. No EC flux could be derived in such periods; however, mean wind speeds from

the Rame Head were used in the evaluation of OVOC mixing ratios.

4.1 Sensible heat and momentum fluxes

Sensible heat flux ($Q_H = \overline{w'T_a'}$) and momentum flux ($\tau = \rho\overline{w'u'}$) were calculated hourly using data from the sonic anemometer, with ρ being the ambient air density. As expected, Q_H generally followed the trend in temperature, higher during the day than at night. Lower Q_H was observed for SSW winds over Plymouth Sound than for W winds over more land. Greater Q_H in the latter case was likely related to concrete buildings and asphalt surfaces within the flux footprint, which absorb and emit heat more quickly than water. The absolute sampling error in Q_H was estimated following Fairall et al. (2000) to be $\sim 30\,\%$ for the daytime.

Momentum flux was generally negative, indicating a transfer of stress to the surface. The friction velocity, $u_* = (-\tau/\rho)^{1/2}$, demonstrated a near-linear relationship with wind speed, but was larger than what is expected over the ocean, likely because of the greater momentum roughness length (z_0) within the flux footprint. Categorizing the region from PML to the water's edge under class 6 for terrain roughness scale (World Meteorological Organization, 2006), z_0 is on the order of 0.5 m. It is uncertain how much the enhanced momentum transfer affected the transfer of scalars, such as heat and OVOCs. To determine atmospheric stability, the Obukhov length was calculated as $L = -u_*^3/[\kappa(g/\theta_v)/Q_H]$. Here κ is the von Karmon constant, g the gravitational acceleration, and θ_v the potential temperature. We take the vertical displacement as half of the height of the roughness elements (5 m), and reference height z the measurement height above displacement (~ 40 m). The Monin–Obukhov stability parameter (z/L) varied from -1 (unstable) to slightly positive (weakly stable) in our observations, with 0 indicating neutrality.

4.2 OVOC fluxes

Precise timing is required for EC to prevent a loss of flux. While the anemometer data were essentially instantaneous, a few seconds were required for air to travel from the inlet to the PTR-MS, through the drift tube, and be detected. Additional time lag may occur due to spatial separation between the wind sensor and the inlet and inaccuracy of the computer clock. The most direct method to account for the total time shift is to perform a lag correlation analysis between OVOC mixing ratio and w.

We linearly interpolated winds at 10 Hz to the sampling frequency of the PTR-MS at 2.1–2.5 Hz. Lag correlations between w and all three OVOC species were calculated hourly within a ± 15 s window. A sharp peak in correlation coefficient indicated a clearly detected flux, with the time of maximum correlation corresponding to the total lag. Methanol flux was always easily detectable, yielding the most robust

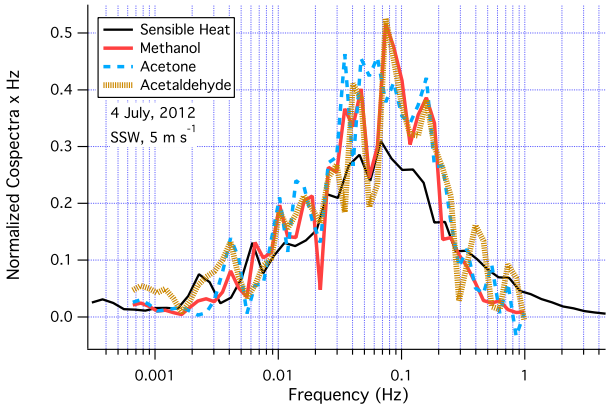

Fig. 5. Cospectra of sensible heat, methanol, acetone, and acetaldehyde normalized to the respective fluxes during 4 h of steady winds on 4 July. Trimming of plants immediately upwind resulted in exceptionally large fluxes and well-defined cospectra for all three OVOC species, which showed good agreement with each other.

lag time estimates at -4.5 ± 0.5 s, consistent with given flow rates. Analogous analyses between w and acetaldehyde or acetone demonstrated clear peaks when the fluxes were large, with lag times in agreement with those between w and methanol. For other hours, lag times from the methanol analysis were used for acetaldehyde and acetone flux calculations. After synchronization, OVOC fluxes were processed in hourly blocks. Periods of rapid change in wind direction or large spikes in mixing ratios were excluded if they occurred at the beginning or end of the analysis window. We did not apply a despiking algorithm on the mixing ratios prior to flux calculation but instead used hourly statistics for quality control, as described in Sect. 4.4.

To examine the robustness of measured fluxes and determine the dominant flux timescale, we compare the cospectra of OVOCs to the cospectrum of sensible heat. Each was normalized by the respective flux and usually averaged over a few hours of steady winds to reduce noise. An example is shown in Fig. 5. Measured coincidentally during and after trimming of garden bushes in the upwind region, the OVOC fluxes were exceptionally large and the cospectra well defined. The four cospectra agreed with each other and demonstrated the expected shape from atmospheric turbulent transport (Kaimal et al., 1972). During our observational period, the methanol cospectrum was almost always well defined and similar to that of sensible heat. Cospectra of acetaldehyde and acetone were noisier because of their lower flux magnitudes.

4.3 Sampling error and precision in OVOC flux

Due to stochastic randomness in turbulent eddies, flux needs to be averaged over a long enough time period (T) to be statistically representative. We estimate the absolute (random)

sampling error in OVOC fluxes (ΔF_C) following Blomquist et al. (2010):

$$\Delta F_c = \frac{a\sigma_W \sigma_{\mathrm{Ca}}}{\sqrt{T/\tau_{W\mathrm{Ca}}}} \left[1 + \frac{\varphi_{\mathrm{Cn}}}{4\sigma_{\mathrm{Ca}}^2 \tau_{W\mathrm{Ca}}} \right]^{1/2}. \quad (4)$$

An expansion of the formulae from Fairall et al. (2000), ΔF_C in Eq. (4) arises from both natural variability (first term on RHS) and instrumental noise (second term on RHS). The natural variance in the OVOC mixing ratio (σ_{Ca}^2) is taken to be the second point in the autocovariance function; a is an empirical constant, while σ_W is the standard deviation in w. The noise contribution relates to the white noise of the instrument (φ_{Cn}), which was about 0.02–0.03 $\mathrm{ppb^2\,Hz^{-1}}$. The integral timescale ($\tau_{W\mathrm{Ca}}$) increases with sampling height and decreases with wind speed:

$$\tau_{W\mathrm{Ca}} = b\frac{z}{u}[\min(5, \max(0.5, (1 + 0.6z/L))]^{-1}. \quad (5)$$

ΔF_C is similar for neutral and unstable cases but amplifies for a stable atmosphere. Using empirical values of 1 and 2.8 for a and b (C. Fairall, unpublished data), the flux sampling error for methanol was on the order of $\sim 50\,\mu\mathrm{mol\,m^{-2}\,d^{-1}}$, or $\sim 30\,\%$ of the mean flux. ΔF_C decreased to $\sim 30\,\mu\mathrm{mol\,m^{-2}\,d^{-1}}$ ($\sim 20\,\%$) at winds above $10\,\mathrm{m\,s^{-1}}$ but increased substantially in calm conditions. For acetaldehyde and acetone, the flux errors averaged ~ 10 and $\sim 16\,\mu\mathrm{mol\,m^{-2}\,d^{-1}}$, or $\sim 70\,\%$ and $50\,\%$ of the mean respective fluxes. Except for in pollution plumes, natural variance was several times smaller than white noise, but contributed to more than half of the sampling error in Eq. (4), which caused ΔF_C to be greater for methanol than for acetaldehyde and acetone.

Spirig et al. (2005) estimated the precision in EC flux from variability of the covariance at a time lag far away from the true lag. We follow the same strategy and calculate "null" OVOC fluxes at an implausible lag time (+15 s). From several hours of steady winds, σ of the null fluxes were ~ 8, 5, and $4\,\mu\mathrm{mol\,m^{-2}\,d^{-1}}$ for methanol, acetaldehyde, and acetone, increasing with natural variance as well as instrumental noise. Estimated as 3σ, the detection limits of our system with respect to these compounds were ~ 24, 15, and $12\,\mu\mathrm{mol\,m^{-2}\,d^{-1}}$ for hourly measurements, on the same order as ΔF_C. In an environment where natural variance is small (e.g., over the ocean), absolute uncertainty in flux should be reduced correspondingly. For the limiting case of σ_{Ca}^2 near 0, Eq. (4) predicts a flux sampling error on the order of $5\sim 10\,\mu\mathrm{mol\,m^{-2}\,d^{-1}}$.

4.4 Quality control filters

Over spatially homogenous terrain and under stationary conditions, horizontal terms in the conservation equation approach zero, allowing measured turbulent transport at height to be equated to surface flux. In reality, these criteria were strictly never satisfied at our location due to variable seascapes and changing meteorological conditions. As a result, we rely on quality control filters based on hourly statistics in winds, turbulence, and OVOC mixing ratios to limit errors arising from nonstationarity and inhomogeneity. Valid heat fluxes must satisfy all of the following: σ in wind direction less than 60°, ratio of horizontal wind variance to wind speed less than $1\,\mathrm{m\,s^{-1}}$, z/L less than 0.05, σ_W/u_* between 1.0 and 1.6, Q_{H} over $-20\,\mathrm{W\,m^{-2}}$, and the difference between covariance- and cospectrum-integrated Q_{H} less than 20 % (for the daytime).

Schulz and Sanderson (2004) used σ in wind direction and the horizontal wind variance as stationarity criteria for analyzing shipboard data. We use the same indicators but relax the thresholds given the more variable winds in our region. Based on EC measurements of DMS over the open ocean, Yang et al. (2011) showed greater uncertainty and possible underestimation of the flux under stable conditions ($z/L < 0.05$), when turbulence becomes more intermittent. A measure of the relative importance between convective and mechanically driven turbulence, σ_W/u_* is expected to be around 1.3 for the surface layer. We interpret σ_W/u_* far from 1.3 to indicate severe flow distortion or suppressed turbulence. Lastly, the integral of the cospectrum over all measured frequencies is mathematically equivalent to the direct covariance. Methodological errors are implied when the covariance and cospectrum-integrated fluxes differ substantially. About 70 % of the hourly heat flux measurements pass the aforementioned filter. Because of the occurrence of stable nocturnal boundary layer, more daytime flux measurements remain valid.

For OVOC fluxes, we require Q_{H} to be valid, and place additional filters on short-term variability and long-term trend in OVOC mixing ratios. Calculated as the hourly σ divided by mean mixing ratio, large short-term variability reflects changes in mixing ratio due to processes other than vertical transport, such as advection of a plume or horizontal turbulent flux arose from inhomogeneity. Nominal criteria are less than 0.8 for methanol and acetaldehyde and less than 0.4 for acetone, the latter a result of its smaller fluctuations. Long-term variability is quantified by the temporal change in OVOC mixing ratio (hourly) divided by the mean, with a threshold set to $0.3\,\mathrm{h^{-1}}$ for all OVOCs. About half of the measured OVOC fluxes pass all aforementioned criteria.

Following Spirig et al. (2005) and Schulz and Sanderson (2004), we further evaluate the stationarity assumption through the ogive analysis (Oncley, 1989). The ogive (Og) is calculated as the cumulative sum of the cospectrum (Co) from the lowest measured frequency (f_{L}) to the Nyquist frequency (f_{N}):

$$\mathrm{Og}(f) = \int_{f_{\mathrm{L}}}^{f_{\mathrm{N}}} \mathrm{Co}(f)\mathrm{d}f. \quad (6)$$

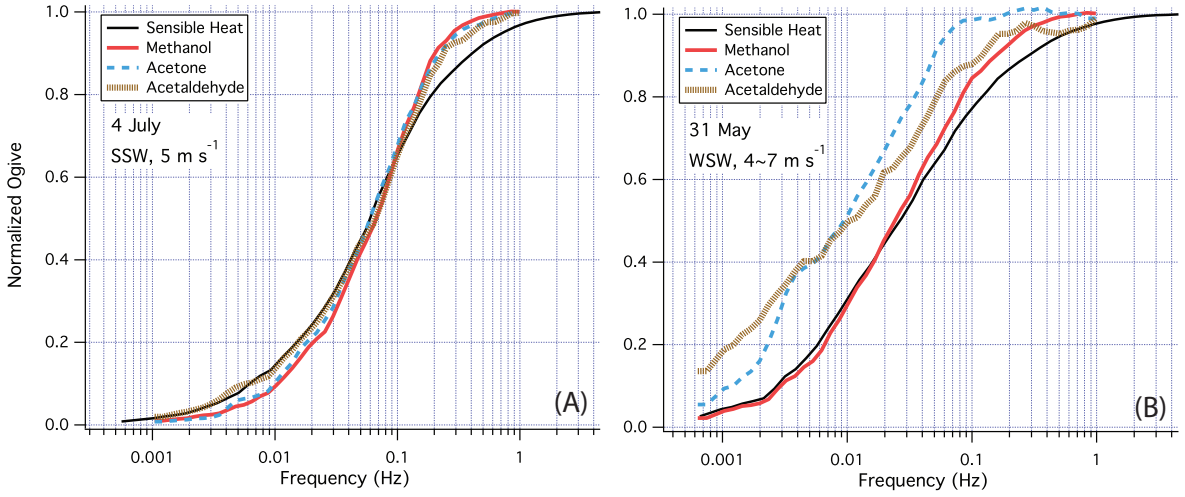

Fig. 6. Ogive of sensible heat, methanol, acetone, and acetaldehyde normalized to the respective fluxes for 4 July **(A)** and 31 May **(B)**. On 4 July (same period as Fig. 5), the ogives of different OVOCs demonstrated good agreement with each other and to that of sensible heat due to strong local emissions and steady winds. In contrast, rising winds on 31 May caused increasing mixing ratios of acetone and acetaldehyde, which is evident in the greater ogives at low frequencies.

For ease of comparison, dividing Eq. (6) by the flux yields a normalized Og of 1 at f_N. Ogives from two periods are shown in Fig. 6. On 4 July, strong surface emissions, steady winds, and well-defined cospectra (Fig. 5) led to the expected "S" shape for all ogives. On 31 May, however, rising winds led to increasing mixing ratios in acetone and acetaldehyde, but not methanol, which are reflected as elevated Og for acetone and acetaldehyde at low frequencies. While it might be easier to satisfy the stationarity requirement by computing flux at shorter intervals (e.g., 15 min), approximately hourly averaging is beneficial for resolving OVOC transport at the given instrumental noise.

4.5 Quantifying flux loss

At high frequencies, flux loss occurs as a result of limited instrument response, which is evident in Fig. 5. The drop off to zero is abrupt in the OVOC cospectra at ~ 1 Hz, whereas a "tail" remained in the sensible heat cospectrum up to 5 Hz. While all four cospectra peaked at ~ 0.07 Hz, OVOCs were normalized to attenuated values and thus demonstrated higher maxima than heat. OVOCs are also often considered "sticky" due to their propensity to adsorb to the tubing wall, which could lead to further flux attenuation.

We estimate flux loss in two ways – from the instrument frequency response and based on concurrent heat flux measurements. Bariteau et al. (2010) parameterized flux loss through tubing using the instrument response time (τ_c), defined as the number of seconds for a pulsed signal to fall to $1/e$ of its original value. An empirical filter function is given the form $H(f) = [1 + (2\pi f \tau_C)^2]^{-1}$. True turbulent flux is then adjusted from measured flux by the factor $H(f)^{-1/2}$. While the theoretical response time of the PTR-MS is quoted to be 0.1 s, the actual response time in our setup appears to be slower. In earlier laboratory tests with identical flows, while sampling at ~ 6 Hz, we injected d_3-methanol standard at the tip of the 25 m inlet and observed the decline of the signal once the standard was turned off by a fast-switching valve; τ_c was determined to be ~ 0.5 s, corresponding to a half-power frequency of ~ 0.3 Hz. Inserting τ_c to the filter function and applying it to the measured cospectra up to f_N resulted in flux corrections on the order of 10–20 %. Estimated from comparison to the Kaimal spectrum, contribution to turbulent flux at frequencies above f_N was small at typically a few percent.

Further loss in OVOC flux could occur as a result of spatial separation between the gas inlet and the sonic anemometer (Moore, 1986). Thus we compare the transport of OVOCs to the transport of heat (which should have negligible attenuation). Instead of matching cospectra, we find the ogive approach for estimating high-frequency attenuation (Spirig et al., 2005; Ammann et al., 2006) to be more repeatable. Averaged over a few hours of relatively constant winds to reduce noise, Og of OVOC usually reached 1 at a lower frequency than the heat ogive, implying high-frequency attenuation. We scaled the OVOC Og to the heat Og up to a frequency where attenuation was not yet significant (usually ~ 0.05 Hz). The corrected OVOC Og at f_N then indicated the magnitude of flux attenuation. Three examples of the ogive analysis for methanol are shown in Fig. 7. On 30 May, 6 June, and 15 June, the wind speeds were about 5, 8, and 11 m s^{-1}, with stability parameter z/L at -0.70, -0.16, and -0.05, respectively. The estimated loss in flux at a sampling rate of 2.1 Hz was ~ 7, 17, and 24 % for these three days, increasing with wind speed and stability, which is caused by greater flux contribution from high frequencies with increasing mechanically driven turbulence. Losses in flux for methanol, acetaldehyde,

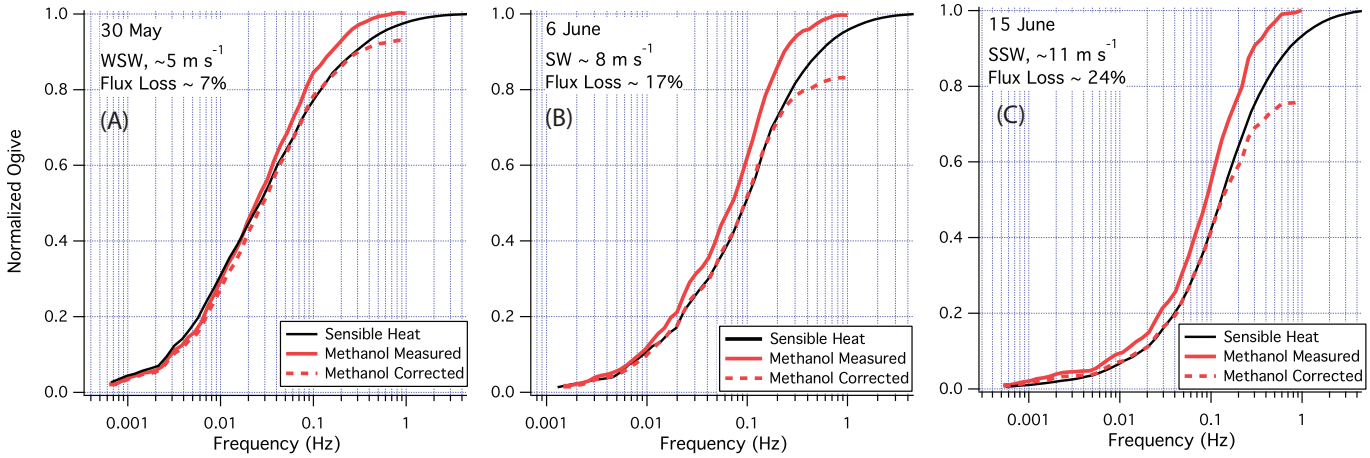

Fig. 7. Ogives of sensible heat and methanol (before and after attenuation correction) for three days of different wind speeds and atmospheric stability. Flux loss at high frequencies increased with wind speed and stability, where a greater contribution to the flux came from smaller eddies.

and acetone based on this analysis are similar to each other and comparable to the filter function estimates, suggesting insignificant roles of adsorption and sensor separation.

Recently, Geissbaum and Schmidt (2009) examined the effect of flow distortion on turbulent measurements from a location of severe wind obstruction (e.g., a heavily instrumented tower). Through 3-D fluid dynamic modeling and large eddy simulation, they found that the double rotation correction for streamline flow could lead to overestimation of scalar fluxes up to 15 %. Such a bias would be similar in magnitude to our frequency-related flux loss, but opposite in direction. Given the flow distortion at our site, we decide to present OVOC fluxes "as measured", rather than applying any correctional factors. Nevertheless, the methods discussed above should be useful for correcting measurements at more ideal locations. Overall, we see that most of turbulent transport can be captured by sampling at a relatively modest rate of > 2 Hz.

5 Results and discussion

Three time periods of flux measurements are shown here to demonstrate the application of quality control filters and the variability in OVOC fluxes. The first is taken from 30 May to 1 June, during three days of largely sunny weather and light westerly breeze. Figure 8 shows time series of wind direction and solar irradiance (A), temperature and sensible heat flux (B), methanol mixing ratio and flux (C), acetaldehyde mixing ratio and flux (D), and acetone mixing ratio and flux (E). We have included fluxes both accepted and rejected by the quality control filters, with error bars corresponding to the absolute flux sampling errors (as with subsequent flux plots). With winds coming over land, methanol mixing ratio was high during this period. Many hours were discarded because of excessive variability in wind direction (usually when winds ceased) or rapidly varying mixing ratios. Within remaining valid data, acetaldehyde flux followed the trend of Q_H, and was slightly positive at night (emission), while acetone flux was usually positive but also occasionally negative (deposition).

The second example is taken from 6 to 8 June (Fig. 9), the same period as Fig. 2. Wind direction was fairly steady from WSW on 6 June and W on 8 June, with mostly sunny weather. Heavy rain fell for most of 7 June and the early morning of 8 June, corrupting sonic anemometer data. Acetaldehyde flux was always positive, ranging from $\sim 30\,\mu mol\,m^{-2}\,d^{-1}$ during the day to lower values in the early morning or late afternoon. Acetone flux was positive under strong sunlight ($\sim 60\,\mu mol\,m^{-2}\,d^{-1}$) but near zero otherwise. The rapid declines in fluxes of sensible heat, acetaldehyde, and acetone on the afternoon of 6 June were probably due to not only diminishing solar irradiance at the end of the day but also a shift in wind direction towards the south. Methanol mixing ratio varied more than an order of magnitude and changed markedly with wind direction. The rapid buildup and large spikes in methanol mixing ratio on 8 June, when acetaldehyde and acetone mixing ratios only increased gradually, suggest different sources and sinks for methanol.

Lastly, Fig. 10 shows the time series during the period 15–16 July. Wind speeds were $\sim 8\,m\,s^{-1}$ the first day and increased to $\sim 11\,m\,s^{-1}$ on the second day, while the weather changed from sunny to mostly cloudy with intermittent showers. A rapid shift in winds occurred from 05:00 to 08:00 on 16 July, accompanied by a 2 °C drop in air temperature and doubling of methanol and acetone mixing ratios, whereas acetaldehyde mixing ratio was less affected. EC fluxes during such hours of rapid changes were rejected, as were hours with large spikes in OVOC mixing ratios (e.g., 14:00–16:00

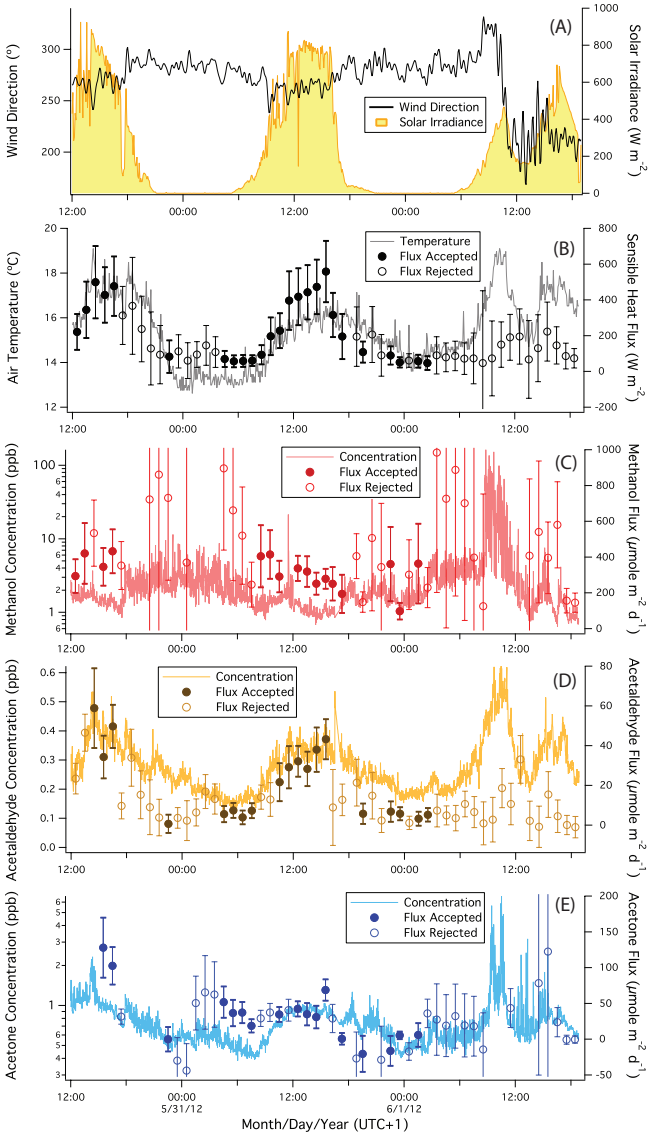

Fig. 8. Time series of wind direction and solar irradiance **(A)**, temperature and sensible heat flux **(B)**, methanol mixing ratio and flux **(C)**, acetaldehyde mixing ratio and flux **(D)**, and acetone mixing ratio and flux **(E)** from 30 May to 1 June, three sunny days with mostly light to moderate breeze from land. Methanol mixing ratio increased by over an order of magnitude when the winds ceased, while acetaldehyde and acetone mixing ratios were generally higher during the day than at night. Many hours of fluxes did not pass the quality control criteria because of excessive variability in wind direction.

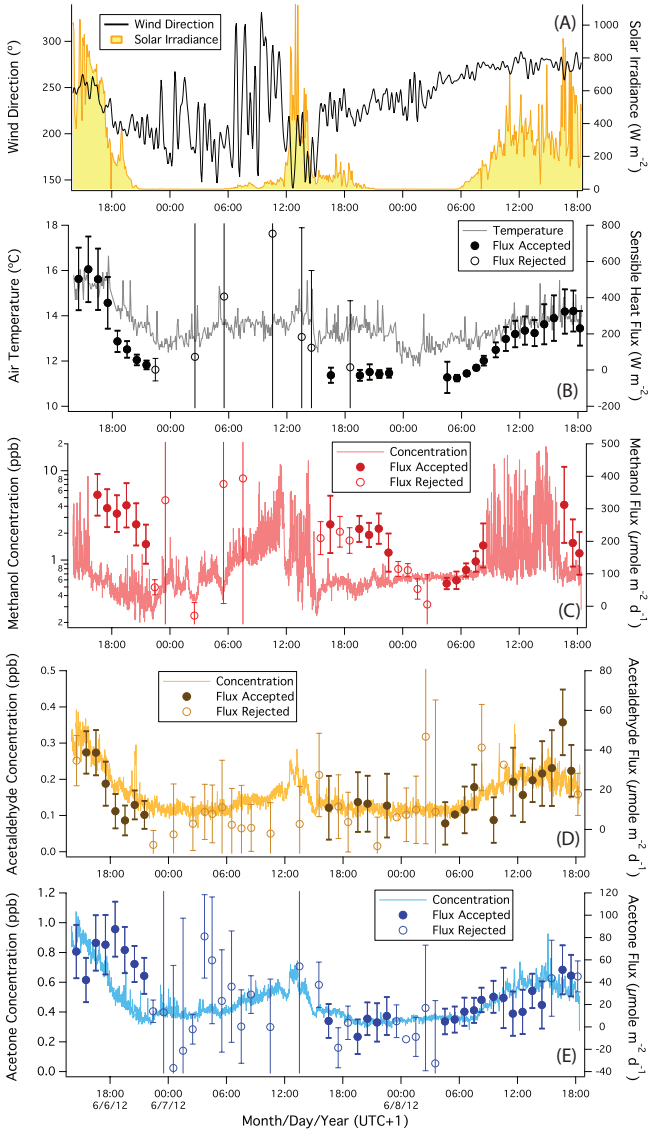

Fig. 9. As with Fig. 8, but for 6–8 June. During this windy period, acetaldehyde and acetone fluxes as well as mixing ratios were higher during the day, following the trend of heat flux. Acceptable flux measurements could not be made for most of 7 June and a few hours on 8 June due to corruption of the sonic anemometer data in the presence of heavy rain.

on 16 July for acetaldehyde). On average, acetaldehyde flux was slightly positive, while acetone flux was near zero for the nighttime. Methanol flux did not demonstrate a clear diel difference, but varied with wind direction.

5.1 General behaviors in OVOC fluxes

In Fig. 11, we plot hourly fluxes of methanol, acetaldehyde, and acetone vs. wind direction. All valid hours from March to July are included here, which are further separated into day and night. Methanol flux was large and always positive, peaking in the direction of WSW. Somewhat higher emissions (mean $\pm 1\sigma$) were observed during the day ($235 \pm 110\,\mu mol\,m^{-2}\,d^{-1}$) than at night ($169 \pm 92\,\mu mol\,m^{-2}\,d^{-1}$) over all wind directions considered; from the direction of Plymouth Sound (SSW) only, flux was

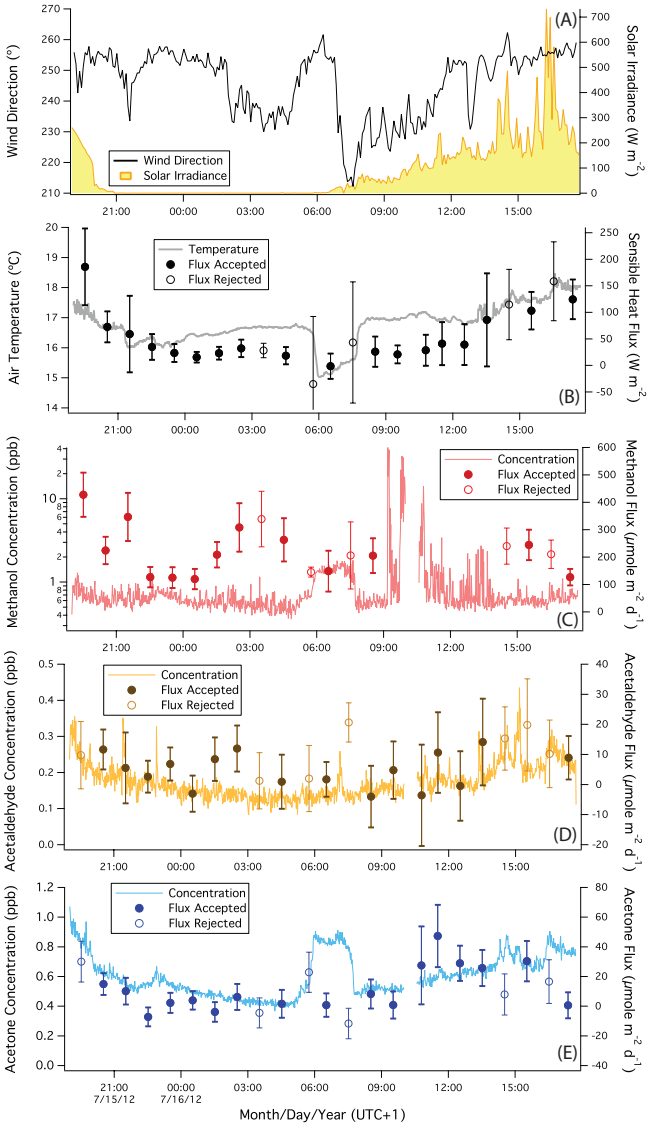

Fig. 10. As with Figs. 8 and 9, but for 15–16 July. Fluxes varied noticeably with wind direction, reflecting an inhomogeneous footprint. A rapid change in wind direction at ∼06:00 on 16 July brought along lower temperature and much higher methanol and acetone mixing ratios. Fluxes were rejected during such periods of highly variable conditions for violation of the stationarity assumption.

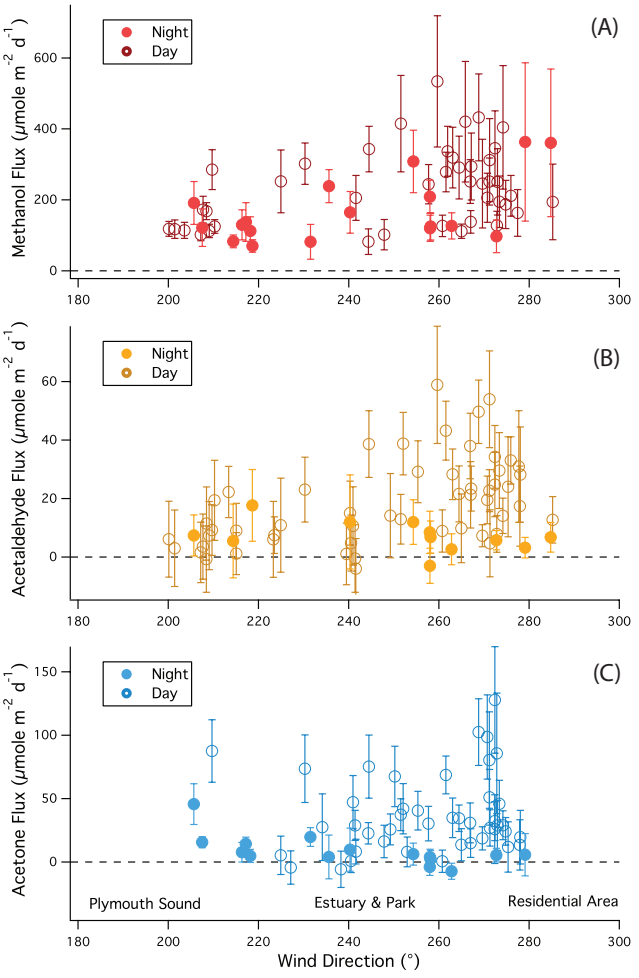

Fig. 11. Hourly fluxes of methanol **(A)**, acetaldehyde **(B)**, and acetone **(C)** from March to July. Methanol fluxes were large and always positive, peaking in the direction of WSW. For acetaldehyde, fluxes were greater during the day than at night for winds over mostly land; from the direction of Plymouth Sound, fluxes were slightly positive and demonstrated little diel difference. Acetone flux was lower at night than during the day, and occasionally negative.

lower and also similar between day and night ($153 \pm 72\ \mu mol\ m^{-2}\ d^{-1}$). For acetaldehyde, much higher flux was observed during the day ($23 \pm 15\ \mu mol\ m^{-2}\ d^{-1}$) than at night ($6 \pm 5\ \mu mol\ m^{-2}\ d^{-1}$) for WSW winds; again no significant diel difference was observed for SSW winds based on limited data ($8 \pm 6\ \mu mol\ m^{-2}\ d^{-1}$). Acetone flux was quite variable but generally larger during the day ($43 \pm 46\ \mu mol\ m^{-2}\ d^{-1}$). With exception of one hour, nighttime acetone fluxes varied between generally $-10\ \mu mol\ m^{-2}\ d^{-1}$ and $20\ \mu mol\ m^{-2}\ d^{-1}$. We can also compare Fig. 11 to the OVOC mixing ratio distributions in Fig. 2, even though the sampling times considered are not identical. For acetaldehyde and acetone, higher fluxes during the day than at night agree with the respective patterns in mixing ratios. For methanol, significant flux at night is consistent with observation of substantial nighttime mixing ratio. Wind directions corresponding to maxima fluxes largely coincide with maxima in mixing ratios, suggesting that the higher daytime mixing ratios were at least in part driven by greater surface emissions.

Diel patterns in OVOC emissions from terrestrial sites have been reported previously based on measurements of fluxes (e.g., Karl et al., 2001; Davison et al., 2009) and mixing ratios (e.g., Hu et al., 2011). Here we demonstrate the relationship between acetaldehyde/acetone flux and the sensible heat flux (Figs. 12 and 13). From the direction of SW

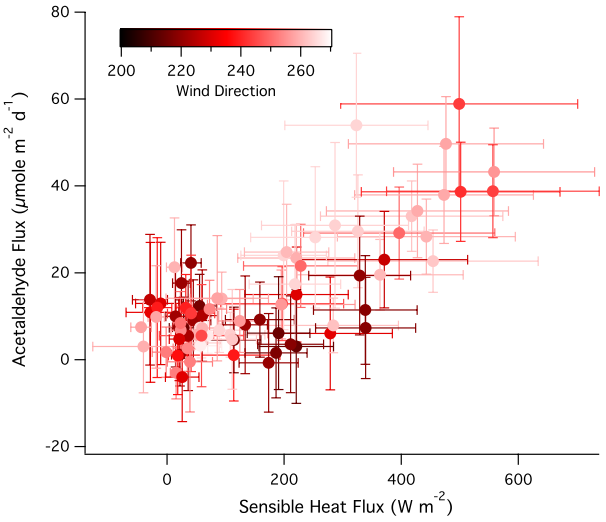

Fig. 12. Acetaldehyde flux vs. heat flux from March to July, color-coded by wind direction. When winds were coming from SW to W, a strong positive correlation was observed between the two fluxes ($r^2 = 0.72$), likely as a result of terrestrial plant emission. With SSW winds, though, acetaldehyde flux was generally lower and demonstrated no clear relationship with heat flux, suggesting possible oceanic emission.

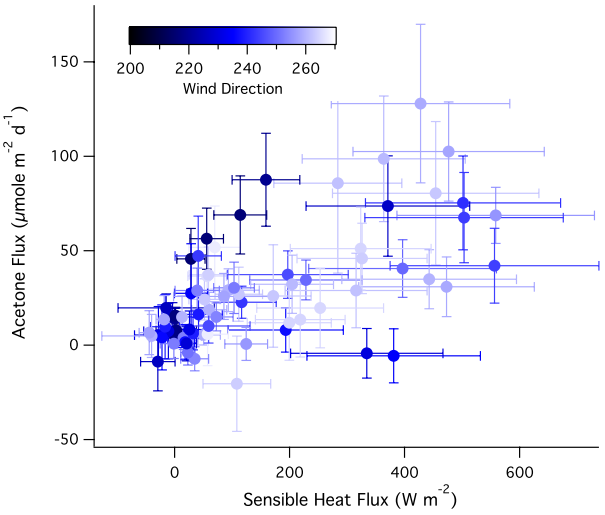

Fig. 13. Acetone flux vs. heat flux from March to July, color-coded by wind direction. A positive correlation was observed between the two fluxes when winds were from the west ($r^2 = 0.52$).

to W, a fairly high degree of correlation exists between acetaldehyde flux and Q_H ($r^2 = 0.72$); in contrast, no correlation is seen in the direction of SSW over Plymouth Sound. A positive correlation also exists between acetone flux and Q_H, in particular when winds were from the W ($r^2 = 0.52$). The same analysis between methanol and Q_H yielded a much weaker correlation ($r^2 = 0.22$), which is not shown here.

Temperature and light dependent, OVOCs are primarily emitted from plant growth in the daytime during photosynthesis, while at night emissions should be reduced due to stomatal control (e.g., Nemecek-Marshall et al., 1995). Given the terrestrial plants present in our flux footprint, positive correlations between OVOC fluxes and sensible heat flux are unsurprising. Interestingly, for the acetaldehyde flux the degree of correlation is higher with Q_H than with temperature, solar flux, or PAR alone. At night, there can still be minor emissions of OVOCs from decaying plants, such as leaf litter. Millet et al. (2010) estimated plant decay to account for about a quarter of the terrestrial plant emission of acetaldehyde globally. Millet et al. (2008) and Jacob et al. (2002) suggested similar fractional contributions by decaying plants to terrestrial emissions of methanol and acetone. Applying this fraction to our daytime fluxes from SW to W yield $\sim 6\,\mu mol\,m^{-2}\,d^{-1}$ of acetaldehyde and $11\,\mu mol\,m^{-2}\,d^{-1}$ of acetone, similar to the mean nighttime fluxes. For methanol, 1/4 of the daytime flux only amounts to $\sim 60\,\mu mol\,m^{-2}\,d^{-1}$, less than half of the nighttime value. Thus, there appear to be other sources of methanol in addition to terrestrial plants, possibly anthropogenic, which would also explain the lower correlation between methanol flux and Q_H. Since our measurements were made during the growing season and from a localized region, actual fractional contributions from plants at night relative to daytime might be significantly different from 1/4.

5.2 Flux and concentration footprints

To better understand the relationship between fluxes and mixing ratios, we must consider their source regions, which are not identical here. The flux footprint describes the horizontal scale (source area) and relative contribution (probability distribution) to the turbulent flux. Elliptical in shape and aligned in the upwind direction from the sensor, the flux footprint varies with measurement height, surface roughness, and atmospheric stability (Horst and Weil, 1992). We estimate our flux footprint using the simple parameterization from Kljun et al. (2004), which relies on u_* and σ_w to describe the stability dependence. The following nominal model inputs were used: z of 40 m, PBL of 1 km, z_0 of 0.5 m, u_* of $0.7\,m\,s^{-1}$, and σ_w of $0.9\,m\,s^{-1}$. The approximate footprints covering cumulative flux contributions of 60 % and 90 % are shown in Fig. 1 for SW winds. The far edge of the footprint at 90 % is about 1 km away from PML, with the peak contribution occurring at ~ 350 m upwind of the sensor, near the waterfront. Lowering σ_W/u_* to 1.0 (more shear) lengthens the footprint by ~ 20 %, while increasing σ_W/u_* to 1.6 (more convection) shortens it by ~ 20 %. With winds from SSW to SW, the relative areal contributions from land and water are on the order of 30 % and 70 %, respectively. Measured flux thus represents the net turbulent transport from within the footprint, or a spatial average of all emissions and depositions.

The source area for mixing ratio (or the concentration footprint) is much larger than the flux footprint (Wilson and Swaters, 1991; Schmid, 1994). Thus changes in mean mixing ratios at the source can be detected at a long distance away, where turbulent flux contribution has already vanished. Large amounts of OVOCs are almost certainly emitted from terrestrial plants in Mount Edgcumbe Park. At ~ 2 km away from PML, the park probably lies beyond the flux footprint, but is well within the concentration footprint. Thus OVOC mixing ratios for SW winds likely reflect emissions within the flux footprint and also from Mount Edgcumbe, which are then advected to our sensor.

5.3 Expected air–sea transfer

To put our measured fluxes in perspective, we use gas exchange parameterizations to approximate the expected air–sea flux based on measured atmospheric mixing ratios at PML (C) and waterside concentrations (C_w) from near Plymouth Sound: $K_\mathrm{a}(C_\mathrm{W}/\alpha - C)$. Here α is the dimensionless solubility, and K_a the total transfer velocity from the air perspective. Following the two-layer model (Liss and Slater, 1974), K_a is expanded to individual transfer velocities through the airside and waterside (k_a and k_w, respectively). For simplicity, we calculate k_a from Duce et al. (1991) and k_w from the NOAA COARE gas transfer model (Fairall et al., 2003, 2011) with a constant of 1.3 for direct transfer and zero for bubble-mediated transfer. At 14 °C and a wind speed of 8 m s^{-1}, K_a for methanol, acetaldehyde, and acetone are on the order of 3100, 2100, and 2300 cm h^{-1}, respectively.

Since waterside OVOC concentrations were not measured concurrently to the EC fluxes, we refer to near-surface (~ 5 m) observations from weekly sampling at the L4 station in 2011. As described in detail by Beale et al. (2011), seawater OVOC concentrations were analyzed with the same PTR-MS coupled with a membrane inlet. For the year 2011, the mean (maximum) seawater concentrations of methanol, acetaldehyde, and acetone from March to July were 50 (68) nM, 9 (19) nM, and 7 (10) nM. We also examined the possible influence of the River Tamar by taking water samples at a depth of ~ 10 cm along a transect from the mouth of Plymouth Sound to the inside of the estuary on the morning of 16 June 2012. Measured at a period of outgoing tide, OVOC concentrations were broadly similar to the springtime values in 2011 and did not show any enhancement inside of the estuary compared to Plymouth Sound.

With nighttime atmospheric mixing ratios of 0.46, 0.13, and 0.39 ppb and the above mean (maximum) waterside values, the expected air–sea fluxes are -10 (-9), 5 (13), and -5 (-4) µmol m^{-2} d^{-1} for methanol, acetaldehyde, and acetone, respectively. The predicted air–sea flux of methanol is much smaller in magnitude and opposite in sign to the measured vertical flux, likely because deposition to the sea surface was overwhelmed by large terrestrial emissions. The expected oceanic emission of acetaldehyde is consistent with the measured flux from the SSW. Though given the heterogeneities within the flux footprint, the possibility of coincidental agreement cannot be ruled out. The predicted air-to-sea flux of acetone is consistent in sign with EC measurements from Marandino et al. (2005) and the recent model estimate from Fischer et al. (2012) for the North Atlantic. While our mean nighttime flux of acetone was slightly positive, negative flux was also occasionally observed and on the order of -5 µmol m^{-2} d^{-1}.

5.4 Photochemistry and local OVOC cycling

In addition to surface emission and deposition, OVOCs are also produced in situ from oxidations of precursors and photochemically destroyed. Here we crudely estimate their photochemical rates and compare them to observed vertical fluxes and time rate of change in mixing ratios. The precursor compounds considered include only the major contributors and do not mean to be exhaustive. The principal atmospheric source of methanol is the reactions of methyl peroxy radical with itself and with other peroxy radicals (Madronich and Calvert, 1990). Acetaldehyde is mainly formed from direct oxidations of alkanes including ethane, propane, and *n*-butane, as well as propene and ethanol by the OH radical (Millet et al., 2010), with oxidation of isoprene through intermediates being a minor source. Acetone is primarily produced from OH oxidation of propane and C_4–C_5 isoalkanes, including mainly *i*-butane and *i*-pentane (Singh et al., 1994).

For precursor mixing ratios, we use 1, 0.1, 0.03, 0.02, and 0.02 ppb for ethane, propane, *n*-butane, *i*-butane, and *i*-pentane from springtime measurements at Mace Head (Grant et al., 2011). From the same location, Salisbury et al. (2001) reported ~ 0.02 ppb of propene and 4 ppt of peroxy radical (an upper limit of organoperoxy radical) in the spring from the ocean sector. Lastly, from mass scans with the PTR-MS, we observed mixing ratios of ethanol and isoprene on the order of 0.1 and 0.04 ppb, respectively. For simplicity, we assume a diel average OH mixing ratio of 10^6 molecules cm^{-3} and the kinetic reaction rates with OH from Sander et al. (2006). The molar yields from precursor compounds are taken from Millet et al. (2008) for methanol, Millet et al. (2010) for acetaldehyde, and Jacob et al. (2002) for acetone.

The estimated methanol production rate from peroxy radical is only 0.009 ppb d^{-1}, much lower than the methanol destruction rate by OH at -0.078 ppb d^{-1} (for 1 ppb of methanol). The photochemical production of acetaldehyde is about 0.06 ppb d^{-1}, while OH oxidizes acetaldehyde at -0.28 ppb d^{-1} (for 0.2 ppb of acetaldehyde). Photochemical production of acetone is about 0.014 ppb d^{-1}, while its loss to OH is also slow at -0.007 ppb d^{-1} (for 0.5 ppb of acetone). Using the absorption cross section and quantum yield from Blitz et al. (2004) and the spectral actinic flux from the NCAR Tropospheric Ultraviolet and Visible (TUV) radiation

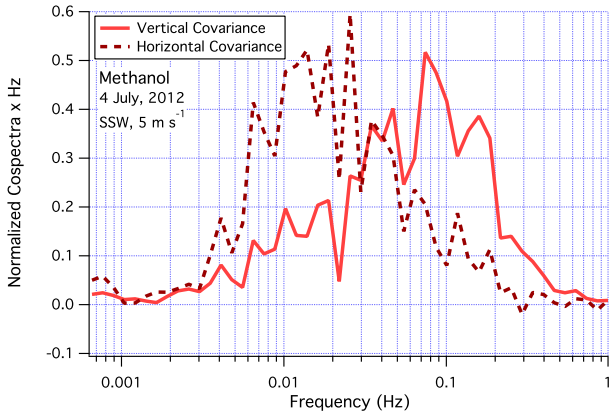

Fig. 14. Normalized methanol cospectra for vertical covariance (same as Fig. 5) and horizontal covariance on 4 July. The horizontal cospectrum peaked at a lower frequency than the vertical cospectrum, likely related to spatial inhomogeneity.

model (http://cprm.acd.ucar.edu/Models/TUV/), we estimate a photolytic loss of acetone of -0.011 ppb d^{-1}.

The net photochemical rates for methanol, acetaldehyde, and acetone are all negative (destruction). In comparison, their average daytime fluxes of 200, 20, 40 µmol m^{-2} d^{-1} into a 1 km thick PBL equate to increases of $\sim$ 2, 0.2, 0.4 ppb over 12 h, suggesting that local emissions contributed significantly to the observed variability of all three OVOCs during the day. At night, the measured fluxes of acetaldehyde and acetone are reduced to $\sim$ 0.06, and 0.1 ppb over 12 h. Compared to their "baseline" (mean nighttime and 1σ) mixing ratios of 0.13 (0.02) and 0.39 (0.08) ppb, local emission appears to be more important for the budget of acetaldehyde than for acetone.

For all three OVOCs, changes in emissions did not always correspond to changes in their mixing ratios. In addition to advection, a part of this apparent imbalance may be explained by the significant horizontal turbulent transport along the mean wind direction ($\overline{u'C'}$), which was usually on the same order as the vertical flux. Compared to the cospectrum of the vertical flux, that of the horizontal turbulent flux was shifted towards lower frequencies, as shown in Fig. 14. The nonzero $\overline{u'C'}$ implies substantial horizontal flux divergence as a result of spatial inhomogeneity, which leads to additional variance in mixing ratio. Such natural variability not only contributes to the random flux sampling error in the vertical and necessitates a longer averaging time (Blomquist et al., 2012), but also could potentially bias the EC measurement judging from studies of sensible heat (Panin et al., 1998; Raabe et al., 2002).

6 Conclusions

In this paper, we characterized the performance of the PTR-MS for measuring fluxes of three OVOCs concurrently with eddy covariance. Total sampling errors and detection limits for hourly fluxes were similar in magnitude; both were determined not only by instrumental noise but also by natural variability in mixing ratios as well as environmental conditions. At a sampling rate of > 2 Hz, high-frequency flux loss was estimated to be 10–20 %, increasing with wind speed and atmospheric stability. Actual uncertainties and biases at our sampling site could be greater due to the distortion of airflow around the building.

Measured OVOC fluxes varied significantly with wind direction and time of day. Higher fluxes of acetaldehyde and acetone were usually observed during the day, peaking in the direction of a forested park. Positive correlations between acetaldehyde flux, acetone flux, and sensible heat flux in the daytime for winds over land were most likely due to emissions from terrestrial plants. From the direction of the sea, however, acetaldehyde flux did not show significant diel difference and largely agreed with the expected sea-to-air transfer. Given its short atmospheric lifetime, the observed nighttime mixing ratio of acetaldehyde was likely sustained in part by marine emission, while contributions from photochemical production appeared to be minor. The small oceanic uptake of acetone predicted is consistent with only some of the observations. The long photochemical lifetime and limited air–sea transport suggest greater role of horizontal advection in the acetone budget. At $\sim$ 200 µmol m^{-2} d^{-1}, methanol emission was about an order of magnitude larger than those of acetaldehyde and acetone. Both the sign and the magnitude of methanol flux were at odds with the expected air–sea transfer, suggesting large terrestrial emission and possibly anthropogenic influence.

This coastal environment is spatially patchy and temporally varying, often resulting in inhomogeneous footprints and nonstationary conditions. Even with careful screening of nonideal sampling conditions, accurate interpretations of measured fluxes are hampered by the complexity of the surroundings. The analytical methods and qualitative relationships between fluxes presented here should be of greater merit than the absolute magnitudes of the fluxes. To more accurately constrain the air–sea exchange of OVOCs, measurements at sea are necessary. The expected magnitudes of air–sea OVOC fluxes are comparable to the instrumental detection limits for hourly flux with reduced natural variance (Sect. 4.3). Thus, future attempts at measuring the fluxes of these OVOCs from a ship will benefit from going to regions of large air/sea concentration differences and high winds.

Note added in proof

After a further 3 months of exposure on the rooftop of PML, the plastic funnel on the front of the gas inlet was taken off and used on a trans-Atlantic research cruise at the end of 2012. The funnel had become brittle and was found to emit contaminants at m/z 45 and 59. The artifact was imperceptible in high latitudes and at night but became severe under intense sunlight in the tropics. It is unknown how the funnel might have affected the acetaldehyde and acetone mixing ratios presented here; due to the relatively low air temperature in Plymouth and the earlier stage of photochemical degradation of the funnel, we suspect the extent of contamination was modest. The measurement of methanol was unaffected. In any case, such an inlet contamination does not alter our suitability analysis of the PTR-MS as a flux instrument.

Acknowledgements. This work is supported by the United States National Science Foundation (grant no. OISE-1064405). The first author would like to thank P. Nightingale and P. Liss for intellectual discussions and hosting, B. Huebert for continued guidance, P. Mason and A. Staff for instrument setup, as well as fellow researchers and staff at PML for assistance. Meteorological data at the Western Channel Observatory are found at http://www.westernchannelobservatory.org.uk/.

Edited by: P. Monks

References

Ammann, C., Brunner, A., Spirig, C., and Neftel, A.: Technical note: Water vapour mixing ratio and flux measurements with PTR-MS, Atmos. Chem. Phys., 6, 4643–4651, doi:10.5194/acp-6-4643-2006, 2006.

Apel, E. C., Brauers, T., Koppmann, R., Bandowe, B., Boßmeyer, J. Holzke, C., Tillmann, R., Wahner, A., Wegener, R., Brunner, A., Jocher, M., Ruuskanen, T., Spirig, C., Steigner, D., Steinbrecher, R., Gomez Alvarez, E., Müller, K., Burrows, J. P., Schade, G., Solomon, S. J., Ladstätter-Weißenmayer, A., Simmonds, P., Young, D., Hopkins, J. R., Lewis, A. C., Legreid, G., Reimann,S., Hansel, A., Wisthaler, A., Blake, R. S., Ellis, A. M., Monks, P. S., and Wyche, K. P.: Intercomparison of oxygenated volatile organic compound measurements at the SAPHIR atmosphere simulation chamber, J. Geophys. Res., 113, D20307, doi:10.1029/2008JD009865, 2008.

Atkinson, R.: Atmospheric chemistry of VOC and NO_x, Atmos. Environ., 34, 2063–2101, 2000.

Bandy, A. R., Thornton, D. C., Blomquist, B. W., Chen, S., Wade, T. P., Ianni, J. C., Mitchell, G. M., and Nadler, W.: Chemistry of dimethylsulfide in the equatorial Pacific atmosphere, Geophys. Res. Lett., 23, 741–744, 1996.

Bariteau, L., Helmig, D., Fairall, C. W., Hare, J. E., Hueber, J., and Lang, E. K.: Determination of oceanic ozone deposition by ship-borne eddy covariance flux measurements, Atmos. Meas. Tech., 3, 441–455, doi:10.5194/amt-3-441-2010, 2010.

Beale, R., Dixon, J., Liss, P., and Nightingale, P.: Quantification of oxygenated volatile organic compounds in seawater by membrane inlet-proton transfer reaction/mass spectrometry, Anal. Chim. Acta, 706, 128–134, 2011.

Blitz, M. A., Heard, D. E., Pilling, M. J., Arnold, S. R., and Chipperfield, M. P.: Pressure and temperature-dependent quantum yields for the photodissociation of acetone between 279 and 327.5 nm, Geophys. Res. Lett., 31, L06111, doi:10.1029/2003GL018793, 2004.

Blomquist, B. W., Huebert, B. J., Fairall, C. W., and Faloona, I. C.: Determining the sea-air flux of dimethylsulfide by eddy correlation using mass spectrometry, Atmos. Meas. Tech., 3, 1–20, doi:10.5194/amt-3-1-2010, 2010.

Blomquist, B. W., Fairall, C. W., Huebert, B. J., and Wilson, S. T.: Direct measurement of the oceanic carbon monoxide flux by eddy correlation, Atmos. Meas. Tech., 5, 3069–3075, doi:10.5194/amt-5-3069-2012, 2012.

Carpenter, L. J., Lewis, A. C., Hopkins, J. R., Read, K. A., Longley, I. D., and Gallagher, M. W.: Uptake of methanol to the North Atlantic Ocean surface, Global Biogeochem. Cy., 18, GB4027, doi:10.1029/2004GB002294, 2004.

Davison, B., Taipale, R., Langford, B., Misztal, P., Fares, S., Matteucci, G., Loreto, F., Cape, J. N., Rinne, J., and Hewitt, C. N.: Mixing ratios and fluxes of biogenic volatile organic compounds above a Mediterranean macchia ecosystem in western Italy, Biogeosciences, 6, 1655–1670, doi:10.5194/bg-6-1655-2009, 2009.

de Gouw, J., Warneke, C., Karl, T., Eerdekens, G., van der Veen, C., and Fall, R.: Sensitivity and speci?city of atmospheric trace gas detection by proton-transfer-reaction mass spectrometry, Int. J. Mass Spectrom., 223–224, 365–382, 2003.

de Gouw, J., Warneke, C., Holzinger, R., Klupfel, T., and Williams, J.: Inter-comparison between airborne measurements of methanol, acetonitrile and acetone using two differently configured PTR-MS instruments, Int. J. Mass Spectrom., 239, 129–137, 2004.

Duce, R. A., Liss, P., Merrill, J. T., Atlas, E. L., Buat-Menard, P., Hicks, B. B., Miller, J. M., Prospero, J. M., Arimoto, R., Church, T. M., Ellis, W., Galloway, J. N., Hansen, L., Jickells, T. D., Knap, A. H., Reinhardt, K. H., Schneider, B., Soudine, A., Tokos, J. J., Tsunogai, S., Wollast, R., and Zhou, M.: The Atmospheric Input of Trace Species to the World Ocean, Global Biogeochem. Cy., 5, 193–259, 1991.

Duncan, B. N., Logan, J. A., Bey, I., Megretskaia, I. A., Yantosca, R. M., Novelli, P. C., Jones, N. B., and Rinsland, C. P.: Global budget of CO, 1988–1997: Source estimates and validation with a global model, J. Geophys. Res., 112, D22301, doi:10.1029/2007JD008459, 2007.

Fairall, C. W., Hare, J. E., Edson, J. B., and McGillis, W.: Parameterization and micrometeorological measurements of air-sea gas transfer, Bound.-Lay. Meteorol., 96, 63- 105, 2000.

Fairall, C. W., Bradley, E. F., Hare, J. E., Grachev, A. A., and Edson J. B.: Bulk parameterization of air-sea fluxes: Updates and verification for the COARE algorithm, J. Climate, 16, 571–591, 2003.

Fairall, C. W., Yang, M., Bariteau, L., Edson, J. B., Helmig, D., McGillis, W., Pezoa, S., Hare, J. E., Huebert, B., and Blomquist, B.: Implementation of the Coupled Ocean-Atmosphere Response Experiment flux algorithm with CO_2, dimethyl sulfide, and O_3, J. Geophys. Res., 116, C00F09, doi:10.1029/2010JC006884, 2011.

Fischer, E. V., Jacob, D. J., Millet, D. B., Yantosca, R. M, and Mao, J.: The role of the ocean in the global

atmospheric budget of acetone, Geophys. Res. Lett., 39, L01807, doi:10.1029/2011GL050086, 2012.

Galbally, I. E. and Kirstine, W.: The production of methanol by flowering plants and the global cycle of methanol, J. Atmos. Chem., 43, 195–229, 2002.

Grant, A., Yates, E. L., Simmonds, P. G., Derwent, R. G., Manning, A. J., Young, D., Shallcross, D. E., and O'Doherty, S.: A five year record of high-frequency in-situ measurements of non-methane hydrocarbons at Mace Head, Ireland, Atmos. Meas. Tech., 4, 955–964, doi:10.5194/amt-4-955-2011, 2011.

Griessbaum, F. and Schmidt, A.: Advanced tilt correction from flow distortion effects on turbulent CO_2 fluxes in complex environments using large eddy simulation, Q. J. Roy. Meteorol. Soc., 135, 1603–1613, doi:10.1002/qj.472, 2009.

Goebbert, D. J. and Wentold, P. G.: Water dimer proton affinity from the kinetic method: dissociation energy of the water dimer, Eur. J. Mass Spectrom., 10, 837–846, 2004.

Guenther, A., Geron, C., Pierce, T., Lamb, B., Harley, P., and Fall, R.: Natural emissions of non-methane volatile organic compounds; carbon monoxide, and oxides of nitrogen from North America, Atmos. Environ., 34, 2205–2230, 2000.

Heikes, B. G., Chang, W. N., Pilson, M. E. Q., Swift, E., Singh, H. B., Guenther, A., Jacob, D. J., Field, B. D., Fall, R., Riemer, D., and Brand, L.: Atmospheric methanol budget and ocean implication, Global Biogeochem. Cy., 16, 1133, doi:10.1029/2002GB001895, 2002.

Horst, T. W. and Weil, J. C.: Footprint Estimation for Scalar Flux Measurements in the Atmospheric Surface Layer, Bound.-Lay. Meteorol., 59, 279–296, 1992.

Hu, L., Millet, D. B., Mohr, M. J., Wells, K. C., Griffis, T. J., and Helmig, D.: Sources and seasonality of atmospheric methanol based on tall tower measurements in the US Upper Midwest, Atmos. Chem. Phys., 11, 11145–11156, doi:10.5194/acp-11-11145-2011, 2011.

Jacob, D. J., Field, B. D., Jin, E. M., Bey, I., Li, Q., Logan, J. A., Yantosca, R. M., and Singh H. B., Atmospheric budget of acetone, J. Geophys. Res., 107, 4100, doi:10.1029/2001JD000694, 2002.

Jacob, D. J., Field, B. D., Li, Q. B., Blake, D. R., de Gouw, J., Warneke, C., Hansel, A., Wisthaler, A., Singh, H. B., and Guenther, A.: Global budget of methanol: Constraints from atmospheric observations, J. Geophys. Res., 110, D08303, doi:10.1029/2004JD005172, 2005.

Jardine, K., Harley, P., Karl, T., Guenther, A., Lerdau, M., and Mak, J. E.: Plant physiological and environmental controls over the exchange of acetaldehyde between forest canopies and the atmosphere, Biogeosciences, 5, 1559–1572, doi:10.5194/bg-5-1559-2008, 2008.

Kaimal, J., Wyngaard, J., Izumi, Y., and Coté, O.: Spectral characteristics of surface layer turbulence, Q. J. Roy. Meteor. Soc., 98, 563–589, doi:10.1002/qj.49709841707, 1972.

Karl, T., Guenther, A., Lindinger, C., Jordan, A., Fall, R., and Lindinger, W.: Eddy covariance measurements of oxygenated volatile organic compound fluxes from crop harvesting using a redesigned proton-transfer-reaction mass spectrometer, J. Geophys. Res., 106, 24157–24167, doi:10.1029/2000JD000112, 2001.

Karl, T. G., Spirig, C., Rinne, J., Stroud, C., Prevost, P., Greenberg, J., Fall, R., and Guenther, A.: Virtual disjunct eddy covariance measurements of organic compound fluxes from a subalpine forest using proton transfer reaction mass spectrometry, Atmos. Chem. Phys., 2, 279–291, doi:10.5194/acp-2-279-2002, 2002

Karl, T., Potosnak, M., Guenther, A., Clark, D., Walker, J., Herrick, J. D., and Geron, C.: Exchange processes of volatile organic compounds above a tropical rain forest: Implications for modeling tropospheric chemistry above dense vegetation, J. Geophys. Res., 109, D18306, doi:10.1029/2004JD004738, 2004.

Kljun, N., Calanca, P., Rotach, M. W., and Schmid, H. P.: A Simple Parameterisation for Flux Footprint Predictions', Bound.-Lay. Meteorol., 112, 503–523, 2004.

Langford, B., Davison, B., Nemitz, E., and Hewitt, C. N.: Mixing ratios and eddy covariance flux measurements of volatile organic compounds from an urban canopy (Manchester, UK), Atmos. Chem. Phys., 9, 1971–1987, doi:10.5194/acp-9-1971-2009, 2009.

Lewis, A. C., Hopkins, J. R., Carpenter, L. J., Stanton, J., Read, K. A., and Pilling, M. J.: Sources and sinks of acetone, methanol, and acetaldehyde in North Atlantic marine air, Atmos. Chem. Phys., 5, 1963–1974, doi:10.5194/acp-5-1963-2005, 2005.

Lindinger, W., Hansel, A., and Jordan, A.: On-line monitoring of volatile organic compounds at pptv levels by means of Proton-Transfer-Reaction Mass Spectrometry (PTR-MS). Medical applications, food control and environmental research, Int. J. Mass Spectrom. Ion Proc., 173, 191–241, 1998.

Liss, P. S. and Slater, P. G.: Flux of gases across the air-sea interface, Nature, 247, 181–184, doi:10.1038/247181a0, 1974.

Madronich, S. and Calvert, J. G.: Permutation reactions of organic peroxy radicals in the troposphere, J. Geophys. Res., 95, 5697–5715, 1990.

Marandino, C. A., De Bruyn, W. J., Miller, S. D., Prather, M. J., and Saltzman, E. S.: Oceanic uptake and the global atmospheric acetone budget, Geophys. Res. Lett., 32, L15806, doi:10.1029/2005GL023285, 2005.

Millet, D. B., Jacob, D. J., Turquety, S., Hudman, R. C., Wu, S., Fried, A., Walega, J., Heikes, B. G., Blake, D. R., Singh, H. B., Anderson, B. E., and Clarke, A. D.: Formaldehyde distribution over North America: Implications for satellite retrievals of formaldehyde columns and isoprene emission, J. Geophys. Res., 111, D24S02, doi:10.1029/2005JD006853, 2006.

Millet, D. B., Jacob, D. J., Custer, T. G., de Gouw, J. A., Goldstein, A. H., Karl, T., Singh, H. B., Sive, B. C., Talbot, R. W., Warneke, C., and Williams, J.: New constraints on terrestrial and oceanic sources of atmospheric methanol, Atmos. Chem. Phys., 8, 6887–6905, doi:10.5194/acp-8-6887-2008, 2008.

Millet, D. B., Guenther, A., Siegel, D. A., Nelson, N. B., Singh, H. B., de Gouw, J. A., Warneke, C., Williams, J., Eerdekens, G., Sinha, V., Karl, T., Flocke, F., Apel, E., Riemer, D. D., Palmer, P. I., and Barkley, M.: Global atmospheric budget of acetaldehyde: 3-D model analysis and constraints from in-situ and satellite observations, Atmos. Chem. Phys., 10, 3405–3425, doi:10.5194/acp-10-3405-2010, 2010.

Moore, C. J.: Frequency response correction for eddy correlation systems, Bound.-Lay. Meteorol., 37, 17–35, 1986.

Nemecek-Marshall, M., Macdonald, R. C., Franzen, F. J., Wojciechowski, C. L., and Fall, R.: Methanol emission from leaves – Enzymatic detection of gas-phase methanol and relation of methanol fluxes to stomatal conductance and leaf development,

Plant Physiol., 108, 1359–1368, 1995.

Northway, M., de Gouw, J., Fahey, D., Gao, R., Warneke, C., Roberts, J., and Flocke, F.: Evaluation of the role of heterogeneous oxidation of alkenes in the detection of atmospheric acetaldehyde, Atmos. Environ., 38, 6017–6028, 2004.

Oncley, S. P.: Flux Parameterisation Techniques in the Atmospheric Surface Layer, Ph.D. thesis, 202 pp., Univ. of California, Irvine, 1989.

Panin, G. N., Tetzlaff, G., and Raabe, A.: Inhomogeneity of the land surface and problem in parametrization of the surface fluxes in natural conditions, Theor. Appl. Climatol., 60, 163–178, 1998.

Raabe, A., Arnold, K., and Ziemann, A.: Horizontal Turbulent Fluxes of Sensible Heat and Horizontal Homogeneity in Micrometeorological Experiments, J. Atmos. Ocean. Tech., 19, 1225–1230, doi:10.1175/1520-0426(2002)019<1225:HTFOSH>2.0.CO;2, 2002.

Rinne, H. J. I., Guenther, A. B., Warneke, C., de Gouw, J. A., and Luxembourg, S. L.: Disjunct eddy covariance technique for trace gas flux measurements, Geophys. Res. Lett., 28, 3139–3142, doi:10.1029/2001GL012900, 2001.

Roberts, J. M.: The atmospheric chemistry of organic nitrates, Atmos. Environ., 24A, 243–287, 1990.

Salisbury, G., Rickard, A. R., Monks, P. S., Allan, B. J., Bauguitte, S., Penkett, S. A., Carslaw, N., Lewis, A. C., Creasey, D. J., Heard, D. E., Jacobs, P. J., and Lee, J. D.:, Production of peroxy radicals at night via reactions of ozone and the nitrate radical in the marine boundary layer, J. Geophys. Res., 106, 12669–12687, doi:10.1029/2000JD900754, 2001.

Sander, S. P., Golden, D. M., Kurylo, M. J., Moortgat, G. K., Wine, P. H., Ravishankara, A. R., Kolb, C. E., Molina, M. J., Finlayson-Pitts, B. J., Huie, R. E., and Orkin, V. L.: Chemical Kinetics and Photochemical Data for Use in Atmospheric Studies, Evaluation Number 15, Jet Propulsion Laboratory, Pasadena, CA, USA, available at: http://jpldataeval.jpl.nasa.gov/, 2006.

Schmid, H. P.: Source areas for scalars and scalar fluxes, Bound.-Lay. Meteorol., 67, 293–318, 1994.

Schulz, E. W. and Sanderson, B. G.: Stationarity of turbulence in light winds during the Maritime Continent Thunderstorm Experiment, Bound.-Lay. Meteorol., 111, 523–541, 2004.

Sinha, V., Williams, J., Meyerhofer, M., Riebesell, U., Paulino, A. I., and Larsen, A.: Air-sea fluxes of methanol, acetone, acetaldehyde, isoprene and DMS from a Norwegian fjord following a phytoplankton bloom in a mesocosm experiment, Atmos. Chem. Phys., 7, 739–755, doi:10.5194/acp-7-739-2007, 2007.

Singh, H. B., O'Hara, D., Herlth, D., Sachse, W., Blake, D. R., Bradshaw, J. D., Kanakidou, M., and Crutzen, P. J.: Acetone in the atmosphere: Distribution, sources and sinks, J. Geophys. Res., 99, 1805–1819, 1994.

Singh, H. B., Kanakidou, M., Crutzen, P. J., and Jacob, D. J.: High mixing ratios and photochemical fate of oxygenated hydrocarbons in the global troposphere, Nature, 378, 50–54, 1995.

Singh, H., Chen, Y., Tabazadeh, A., Fukui, Y., Bey, I., Yantosca, R., Jacob, D., Arnold, F., Wohlfrom, K., Atlas, E., Flocke, F., Blake, D., Blake, N., Heikes, B., Snow, J., Talbot, R., Gregory, G., Sachse, G., Vay, S., and Kondo, Y.: Distribution and fate of selected oxygenated organic species in the troposphere and lower stratosphere over the Atlantic, J. Geophys. Res., 105, 3795–3805, 2000.

Singh, H. B., Salas, L. J., Chatfield, R. B., Czech, E., Fried, A., Walega, J., Evans, M. J., Field, B. D., Jacob, D. J., Blake, D., Heikes, B., Talbot, R., Sachse, G., Crawford, J. H., Avery, M. A., Sandholm, S., and Fuelberg, H.: Analysis of the atmospheric distribution, sources, and sinks of oxygenated volatile organic chemicals based on measurements over the Pacific during TRACE-P, J. Geophys. Res., 109, D15S07, doi:10.1029/2003JD003883, 2004.

Spirig, C., Neftel, A., Ammann, C., Dommen, J., Grabmer, W., Thielmann, A., Schaub, A., Beauchamp, J., Wisthaler, A., and Hansel, A.: Eddy covariance flux measurements of biogenic VOCs during ECHO 2003 using proton transfer reaction mass spectrometry, Atmos. Chem. Phys., 5, 465–481, doi:10.5194/acp-5-465-2005, 2005.

Taddei, S., Toscano, P., Gioli, B., Matese, A., Miglietta, F., Vaccari, F. P., Zaldei, A., Custer, T., and Williams, J.: Carbon dioxide and acetone air-sea fluxes over the Southern Atlantic, Environ. Sci. Technol., 43, 5218–5222, 2009.

Taipale, R., Ruuskanen, T. M., Rinne, J., Kajos, M. K., Hakola, H., Pohja, T., and Kulmala, M.: Technical Note: Quantitative long-term measurements of VOC mixing ratios by PTR-MS – measurement, calibration, and volume mixing ratio calculation methods, Atmos. Chem. Phys., 8, 6681–6698, doi:10.5194/acp-8-6681-2008, 2008.

Warneke, C., Karl, T., Judmaier, H., Hansel, A., Jordan, A., Lindinger, W., and Crutzen, P. J.: Acetone, methanol, and other partially oxidized volatile organic emissions from dead plant matter by abiological processes: Significance for atmospheric HO_x chemistry, Global Biogeochem. Cy., 13, 9–17, 1999.

Warneke, C., Luxembourg, S. L., de Gouw, J. A., Rinne, H. J. I., Guenther, A. B., and Fall, R.: Disjunct eddy covariance measurements of oxygenated volatile organic compounds fluxes from an alfalfa field before and after cutting, J. Geophys. Res., 107, 4067, doi:10.1029/2001JD000594, 2002.

Warneke, C., de Gouw, J. A., Kuster, W. C., Goldan, P. D., and Fall, R.: Validation of atmospheric VOC measurements by proton-transfer-reaction mass spectrometry using a gas chromatographic preseparation method, Environ. Sci. Technol., 37, 2494–2501, 2003.

Williams, J., Holzinger, R., Gros, V., Xu, X., Atlas, E., and Wallace, D. W. R.: Measurements of organic species in air and seawater from the tropical Atlantic, Geophys. Res. Lett., 31, L23S06, doi:10.1029/2004GL020012, 2004.

Wilson, J. D. and Swaters, G. E.: The Source Area Influencing a Measurement in the Planetary Boundary Layer: The "Footprint" and the "Distribution of Contact Distance", Bound.-Lay. Meteorol., 55, 25–46, 1991.

World Meteorological Organization: Initial guidance to obtain representative meteorological observations at urban sites, Instruments and observing methods, Report No. 81, WMO/TD-No. 1250, Geneva, 47 pp., 2006.

Wróblewski, T., Ziemczonek, L., Alhasan, A. M., and Karwasz, G. P.: *Ab initio* and density functional theory calculations of proton affinities for volatile organic compounds, Eur. Phys. J. Special Topics, 144, 191–195, doi:10.1140/epjst/e2007-00126-7, 2007.

Yang, M., Blomquist, B. W., and Huebert, B. J.: Constraining the mixing ratio of the hydroxyl radical in a stratocumulus-topped marine boundary layer from sea-to-air eddy covariance flux measurements of dimethylsulfide, Atmos. Chem. Phys., 9, 9225–

9236, doi:10.5194/acp-9-9225-2009, 2009.

Yang, M., Blomquist, B. W., Fairall, C. W., Archer, S. D., and Huebert, B. J.: Air-sea exchange of dimethylsulfide in the Southern Ocean: Measurements from SO GasEx compared to temperate and tropical regions, J. Geophys. Res., 116, C00F05, doi:10.1029/2010JC006526, 2011.

Zhao, J. and Zhang, R. Y.: Proton transfer reaction rate constants between hydronium ion (H_3O^+) and volatile organic compounds, Atmos. Environ., 38, 2177–2185, 2004.

Zhou, X. and Mopper, K.: Carbonyl compounds in the lower marine troposphere over the Caribbean Sea and Bahamas, J. Geophys. Res.-Atmos., 98, 2385–2392, 1993.